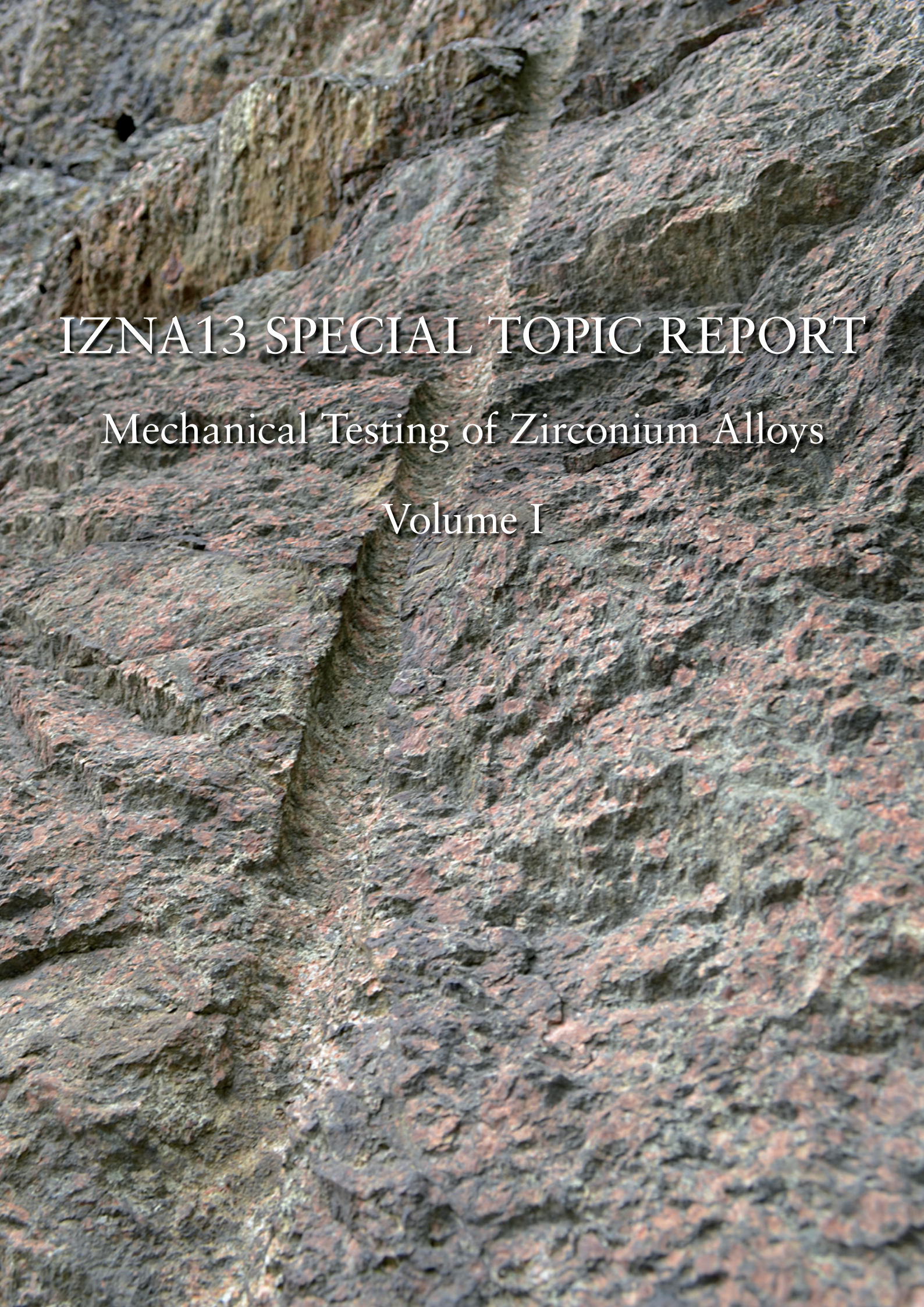

IZNA13 SPECIAL TOPIC REPORT

Mechanical Testing of Zirconium Alloys

Volume I

Mechanical Testing of Zirconium Alloys

Volume I

Authors

Ron Adamson
Fremont, CA, USA

Kit Coleman
Deep River, ON, Canada

Tahir Mahmood
Pleasanton, CA, USA

Peter Rudling
ANT International, Mölnlycke, Sweden

Technical Editor

Ron Adamson
Fremont, CA, USA

A.N.T. INTERNATIONAL®

Advanced Nuclear Technology International
Analysvägen 5, SE-435 33 Mölnlycke
Sweden

info@antinternational.com
www.antinternational.com

Disclaimer

The information presented in this report has been compiled and analysed by Advanced Nuclear Technology International Europe AB (ANT International®) and its subcontractors. ANT International has exercised due diligence in this work, but does not warrant the accuracy or completeness of the information. ANT International does not assume any responsibility for any consequences as a result of the use of the information for any party, except a warranty for reasonable technical skill, which is limited to the amount paid for this assignment by each ZIRAT/IZNA programme member.

Contents

1 Introduction (Ron Adamson)

Mechanical testing of zirconium alloys has many uses: to confirm that the material meets the specification, to evaluate new alloys or modifications to old ones, to elucidate mechanisms of strengthening or embrittlement, and to assess the effects of reactor operation. The mechanical response of any material depends on several different parameters such as:

1) Specimen geometry,
2) Alloy composition and microstructure,
3) Loading conditions such as stress state and strain rate, and
4) Environment such as temperature, irradiation and ambient chemistry.

Residence in a nuclear reactor presents a severe test for materials. Before evaluating the mechanical properties, knowledge is required on the conditions of normal reactor service with its operational variations, the challenge when spent fuel is stored, and the consequences of accidents. Various mechanical tests are done to simulate the conditions faced by fuel cladding and structural components in the reactor. In applying the results from mechanical testing of zirconium alloys to reactor performance, it is crucial to have a good knowledge of the situation being addressed and how the different critical testing parameters affect the material response so the results are useful to predict performance accurately and satisfy regulatory requirements. The objective of this STR in two volumes is to provide this knowledge.

This report is Volume 1 of a two-part Special Technical Report (STR) on mechanical testing of zirconium alloys. Volume 1 deals with separate effects testing, and volume 2 deals with integral or specific phenomena testing. Background information will be included where appropriate, but an extensive literature review of specific performance is not intended.

1.1 Fuel design requirements (Peter Rudling)

The objectives of the *fuel system* safety review are to provide assurance that:

1) The *fuel system* is *not damaged* as a result of normal operation and AOOs.
    a) Fuel system consists of assemblies of fuel rods including fuel pellets, insulator pellets, springs, tubular cladding, end closures, hydrogen getters, and fill gas; burnable poison rods including components similar to those in fuel rods; holddown spring, connections, spacer grids and springs; end plates; channel boxes; and reactivity control elements that extend from the coupling interface of the control rod drive mechanism in the core.
    b) Not damaged means not only that the fuel integrity is maintained, i.e., no release of radioactivity, but also that the fuel system dimensions remain within operational tolerances, and that functional capabilities are not reduced below those assumed in the safety analysis. This objective implements General Design Criterion 10 (GDC10) and the design limits that accomplish this are called Specific Acceptable Fuel Design Limits (SAFDLs).
2) *Fuel system* damage is never so severe as to prevent control rod insertion when it is required.
3) The number of *fuel rod failures* is not underestimated for postulated accidents.
    a) Fuel rod failure means that the fuel cladding has been breached and radioactivity from the fuel get access to the coolant.
4) *Coolability* is always maintained.
    a) Coolability means that the FA retains its rod-bundle geometry with adequate coolant to permit removal of residual heat even after a severe accident.

Objective (1) in the above list is formalized in GDC10 [10 CFR Part 50 Appendix A, 1990]. The application of GDC10 is described in the SRP [USNRC, 2007]. The *fuel system,* nuclear, and thermal and hydraulic designs are covered in SRP Sections 4.2, 4.3 and 4.4, respectively. Section 4.2 in SRP identifies a number of *fuel system* failure mechanisms that actually have occurred in commercial reactors, as well as hypothesized *fuel system* failure mechanisms. For each of these *fuel system* failure mechanisms, SRP Section 4.2 lists a corresponding design limit intended to accomplish objective (1) in the list above. These design limits are called SAFDLs. Thus, the SRP does not include any design limits to address potential new *fuel system* failure mechanisms related to more recent fuel designs and/or reactor operation strategies.

Fuel rod failures must be accounted for in the dose analysis required by 10 CFR Part 100, 1995], for postulated accidents.

The general requirements to maintain control rod insertability and core coolability appear in the General Design Criteria, e.g., GDC 27 and GDC 35. Specific coolability requirements for the loss of coolant accidents, LOCA, are provided in [10 CFR Part 50, §50.46][1].

The *fuel system* design bases must take the four objectives described on the previous page into account. The SAFDLs discussed below do this. In a few cases the SAFDLs provide the design limit but in most cases it is up to the fuel vendor to recommend a design limit value, taking a specific failure mechanism into account. The fuel vendor must also provide the background data for the design limits (that are specified by the NRC as well as those used by the specific fuel vendor) to ensure that the design limit is both necessary and sufficient. The fuel vendor must also provide data for the specific fuel design that shows that the design limit is met to get their fuel licensed.

Specific failure mechanisms for the *fuel system (including the fuel rod)* and licensing criteria related to classes I and II operation and classes III and IV events are discussed in the following subsections.

The pertinent mechanical tests related to fabrication and in-pile performance issues are summarised in Table 1-1. These mechanical tests will be discussed in detail in the following sections of the report.

In the following Section 1.2, only the design criteria related to mechanical properties of the zirconium alloy fuel components are discussed during normal operation and AOO, DBA and Dry Storage.

[1] 10 CFR Part 50, §50.46, *Acceptance criteria for emergency core cooling systems for light water nuclear power reactors*, NRC: http://www.nrc.gov/reading-rm/doc-collections/cfr/part050/

Table 1-1: Relevant mechanical tests for fabrication and in-pile performance issues

	Fabrication Issues		In-Pile Issues	
Component	**Operation**	**Properties**	**Service Condition**	**Property**
Spacer	Bend Punch Cold roll	UE[2], TE[3] UE, TE UE, FT	Seismic, Handling Vibration Dimensions	IS[4], TE, FT[5] F[6], H[7] IG[8]
Channel	Bend Cold roll	UE, TE UE, TE, FT	Seismic, Handling Vibration Wear	IS TE, FT IS TE, FT F H
Water rod/guide tube	Cold reduce	UE, TE, FT	Handling Assembly support	TE, S[9], IS, FT S, TE, FT
Spacer (grid) spring	Cold roll	TE, UE	Vibration Wear Relaxation	F H IG, C[10]
Tubing	Cold roll	TE, UE, FT	Thermal stress PCI Length, bow Differential pressure	F UW, IGSCC[11], LME[12] IG, C, S S, C, UE, B[13]
				ANT International, 2013

[2] Uniform elongation
[3] Total elongation
[4] Impact strength
[5] Fracture toughness
[6] Fatigue
[7] Hardness
[8] Irradiation growth
[9] Strength
[10] Creep
[11] Iodine assisted stress corrosion cracking
[12] Cadmium liquid metal embrittlement
[13] Burst strength

1.2 Normal operation and Anticipated Operational Occurrences (AOO) (Peter Rudling)

1.2.1 Fuel system damage

A fuel component is considered as failed according to SRP if the component does not comply with the fuel design criteria. Thus, a fuel assembly that exhibits more dimensional changes than the fuel design criterion on dimensional stability specifies, the fuel assembly is considered as failed even though the fuel rods may be intact.

1.2.1.1 Stress, strain or loading limits

Stress, strain and loads must be limited for space grids, guide tubes, fuel rods, control rods, channel boxes and other *fuel system* structural members or otherwise the component may fail. Stress limits that are obtained by methods similar to those given in Section III of the ASME Code, see Section 1.2.1.1, [ASME, 2010] are acceptable. Other proposed limits must be justified.

1.2.1.1.1 Stress limit

Plastic deformation is regarded as material failure according to the ASME Code, and must therefore not occur. *This requirement is fictitious since creep deformation is plastic deformation and creep limited strain is allowed.*

Stresses in the *fuel system* structural members may be categorised depending on the origin of the stress and on the geometrical and material discontinuities at the point in the *fuel system* structural member where the stress is calculated.

The ASME Code and comparable design verification systems describe what category of stresses must be taken into account and also how the equivalent stress for each stress category should be evaluated. The design verification systems also specify the maximum allowable equivalent stress in each stress category. The following stress categories, C_i, are defined according to the ASME, [ASME, 2010], and KTA, [KTA, 2013[14]], design specifications.

$C_1 = P_m$ = Primary Membrane Stress

Primary stresses are stresses originating from applied loads such as e.g. cladding stresses due to a fuel rod internal overpressure. Primary stresses are not self-limiting and if the yield stress in the component is exceeded, plastic deformation in the whole material thickness will occur. In the case of a fuel rod this would mean that the whole cladding thickness would plastically deform.

Membrane stress are stresses which have a constant value in the whole material thickness, which means that if the yield stress is exceeded, plastic deformation will occur simultaneously in the whole material thickness.

$C_2 = P_m + P_b$ = Primary Membrane + Primary Bending Stress

Bending stresses will result in varying stress levels in the material thickness and when the yield strength is exceeded only local plastic deformation occurs.

[14] http://www.kta-gs.de/d/regeln/3100/3103_re_2012_11.pdf

$C_3 = P_m + P_b + Q$ = Primary and Secondary Membrane + Bending Stress

Secondary stresses relates to stresses resulting from incompatibility between different volume elements in a component, e.g., caused by a radial temperature gradient in the fuel rod cladding. The secondary stresses are self-limiting, i.e., the stress will relax if the yield strength is exceeded casing the material to locally plastically deform. Examples of secondary stresses are thermal and bending stresses.

The Japanese Guidebook of Safety Assessment and Review, JGSAR, [Motta, 1995] define the following stress categories:

C_1 = Primary Stress

C_2 = Secondary Stress

According to the ASME Code, the Tresca formula should be used to calculate the equivalent stress as follows:

$$\sigma_e = \max\left(\left|\sigma_{11} - \sigma_{22}\right|, \left|\sigma_{22} - \sigma_{33}\right|, \left|\sigma_{33} - \sigma_{11}\right|\right)$$

where

σ_{11}, σ_{22}, σ_{33} are the principal stresses, see Section 2.1.2.

However, according to the KTA and JGSAR Codes of design, the equivalent stress shall be calculated by the von Mises formula, as follows:

$$\sigma_e = \frac{1}{\sqrt{2}}\left[\left(\sigma_{11} - \sigma_{22}\right)^2 + \left(\sigma_{22} - \sigma_{33}\right)^2 + \left(\sigma_{33} - \sigma_{11}\right)^{\frac{1}{2}}\right]$$

For each stress category C_i, let the allowable stress be given by S_i and let Y(T) and U(T) represent the yield strength and the ultimate strength in unirradiated condition, respectively.

The KTA Code specifies that

$$S_1 = \min\left(0.90Y(T), 0.5U(T)\right)$$
$$S_2 = \min\left(1.35Y(T), 0.7U(T)\right)$$
$$S_3 = \min\left(0.90Y(T), 0.50U(T)\right)$$

S_3 =min (2.7Y(T), 1.0U(T)

and the ASME Code states that

$$\begin{matrix} S_1 = 1.0S_m \\ S_2 = 1.5S_m \\ S_3 = 3.0S_m \end{matrix} \text{ where } S_m = \min\left(\begin{matrix} Y(T_0)/1.5 \\ Y(T)/1.5 \\ U(T_0)/3 \\ U(T)/3 \end{matrix}\right) \text{ and } T_0 = 20^oC$$

while the JGSAR design specification requires that

$$S_1 = Y(T)$$
$$S_2 = U(T)$$

The design specification then states that the equivalent stress of the combination of the different stresses σ_e^{max} in a given stress category C_i must not exceed the maximum allowable stress S_i for the particular stress category, i.e.,

$$\left(\sigma_e^{max}\right)_{C_i} \leq S_i$$

It is important to keep in mind that this design stress criterion is very conservative since material properties in unirradiated condition must be used in the above described calculations. However, the yield strength and the ultimate strength material values are dramatically increased during the first couple of months of irradiation, thus increasing the margin on the maximum allowable stress (Figure 1-1).

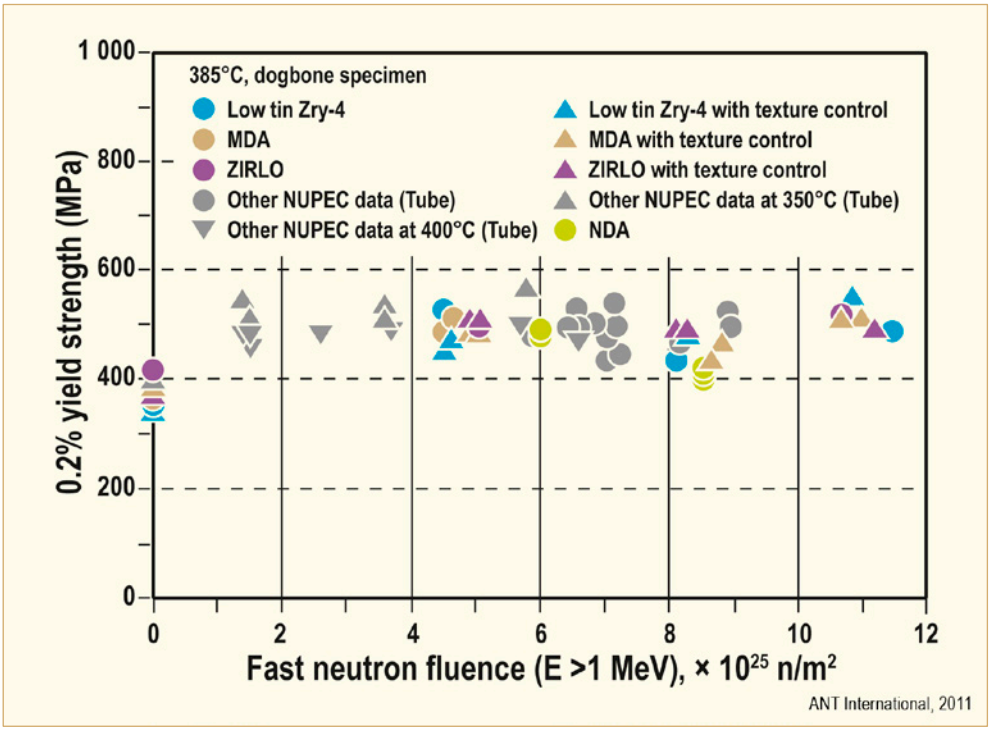

Figure 1-1: Relation between fast neutron fluence and yield strength at 385°C for various Nb-containing and Zry alloys. A fast neutron fluence of $2 \cdot 10^{25}$ n/m^2 corresponds to a burnup of about 5 GWd/MT, after [Tsukuda et al, 2003] and [Goto et al, 2000].

This design stress criterion is the reason for selecting a higher strength fuel cladding material for PWRs compared with BWRs. The fuel cladding stresses are much higher in the former case due to a larger system-rod differential pressure. Therefore, Stress Relieved Cladding, SR, Zry-4 or Zry-2 with a much higher strength was needed historically in PWRs while a softer, Recrystallized, RX, material could be used for BWRs. Since Nb additions to Zirconium have a significant solution hardening effect[15], materials such as M5, Zr1Nb, can be used in PWRs in the RX state.

[15] 40 MPa/% Nb, independent of T.

1.2.1.1.2 Strain limit

At stresses below the yield strength, the material may deform during irradiation due to creep deformation. The SR does not specify a specific creep strain limit.

Design criterion – For BWR fuel rods a maximum allowable equivalent plastic creep strain of 2.5%, corresponding to about 1.5% plastic tangential strain, is sometimes used by fuel vendors (in Germany and Sweden). The initial creep down of the cladding due to larger system than rod internal pressure is not taken into account. Only the outward creep strain after pellet/cladding contact has occurred is compared to the limit. This outward creep is due to pellet swelling during irradiation and occurs at a very slow rate.

For PWRs a maximum allowable creep strain corresponding to a 1% increase in fuel rod diameter compared to the initial diameter is often used (for example, in Sweden, France, the Netherlands, and Switzerland). This limit is related to the risk of getting DNB if the diameter increase becomes too large to permit the coolant to effectively remove heat from the fuel rod; i.e., a small change comes from CHF $\propto (D_{rod})^{-0.5}$, so that a 1% increase in diameter corresponds to about a 0.5% decrease in CHF, while larger changes are postulated to result from cladding deformation due to lift-off, disruption of heat transfer and the propagation of DNB and lift-off conditions among adjacent fuel rods.

1.2.1.2 Fatigue limit

Fatigue stresses may be induced in the fuel assembly components due to, e.g., the turbulent coolant flow.

According to the SRP, the cumulative number of strain fatigue cycles on the structural components should be significantly less than the design fatigue lifetime, which is based upon the data by O'Donnell and Langer, [O'Donnell & Langer, 1964], and includes a safety factor of 2 on stress amplitude or a safety factor of 20 on the number of cycles. Other proposed limits may be used but must be justified according to the SRP.

In design calculations the fuel vendor must show that alternating bending stresses due to dynamic loads must be below $\pm$ 50 MPa.

Normally the dynamic stress is much below $\pm$ 50 MPa in the structural components and therefore there is a lot of safety margin regarding fatigue failures.

1.2.2 Fuel rod failure

SRP states that to meet the requirements of:

- GDC10 as it relates to SAFDLs for normal operation and anticipated operational occurrences and,
- 10CFR Part 100 as it relates to fission product release for postulated accidents,

fuel rod design criteria should be given for all known *fuel rod failure*[16] mechanisms.

[16] Fuel rod failure occurs when the fuel cladding has lost its integrity and radioactive fission products may be released to the coolant.

Different *fuel rod failure* mechanisms that are related to mechanical properties of the claddings are discussed in the following. As was the case for the fuel systems, it is mostly up to the fuel vendor to define a criterion for each fuel rod failure mechanism listed in the SRP to ensure that this failure mechanism will not occur during normal operation and anticipated operational occurrences. In some cases SRP provides the fuel rod design criterion.

1.2.2.1 Cladding collapse

At the start of irradiation the system pressure is larger than the rod internal pressure, resulting in compressive stresses in the fuel cladding. If these stresses become large enough, the cladding tube may either instantaneously buckle elastically or, if the stresses exceed the yield strength, collapse due to plastic deformation. To prevent elastic buckling and plastic deformation, the fuel vendor has to show by calculations that the fuel cladding stresses are below those resulting in elastic buckling or plastic deformation. Fuel rod failure due to elastic buckling or plastic collapse has never been observed in commercial nuclear reactors. A more limiting condition that has been observed in commercial PWR nuclear reactors is cladding creep collapse. This condition occurs at cladding stresses far below that required for elastic buckling or plastic deformation.

In the early 1970s, excessive in-reactor fuel pellet densification resulted in the production of large fuel column pellet-pellet axial gaps in some PWR fuel rods. The high PWR coolant pressure in conjunction with the thin PWR cladding tubes and low fill gas pressure resulted in excessive fuel rod cladding creep rates and subsequent cladding collapse over fuel column axial gaps. Such collapse occurs due to a slow increase of cladding initial ovality due to the cladding creep noted above. The creep results from the combined effect of reactor coolant pressure, temperature and fast neutron flux on the cladding over the axial gap. Since the cladding is unsupported by fuel pellets in the axial gap region, the ovality can become large enough to result in elastic instability and cladding collapse.

While axial gaps can be prevented (or detected) in as-fabricated fuel, the potential formation of gaps during operation cannot be controlled. Thus the vendor must show that the fuel cladding will not collapse, either elastically, plastically or by creep. Elastic and plastic collapse is most limiting at Beginning of Life (BOL) before irradiation hardening of the cladding. Creep collapse becomes limiting later in life.

According to the SRP, a collapsed cladding must be regarded as a failed fuel rod due to the large strains that result from cladding collapse.

Note that in CANDU reactors the Zircaloy-4 fuel cladding is designed to collapse onto the fuel to provide good heat-transfer to the heat-transport heavy water. In this fuel the filler gas, He, is initially at atmospheric pressure.

1.2.2.2 Pellet/Cladding Interaction, PCI

According to the SRP, there is no current criterion for fuel failure resulting from PCI. Two related criteria should be applied, but they are not sufficient to preclude PCI failures:

- The transient induced uniform elastic and plastic strain should not exceed 1%. Since PCI failures may occur at lower strains than 1 %, this criterion is not sufficient to ensure the non-occurrence of PCI failures. The basis for the 1 % criterion is unknown, even to the R&D branch of NRC, [Meyer, 1999].

- Fuel pellet melting should be avoided.

2 Basics

2.1 Basic deformation concepts

2.1.1 Stress and strain in uniaxial tension (Ron Adamson)

Deformation is a change in the shape or size of an object due to an applied force. The deformation can be a result of tensile (pulling) forces, compressive (pushing) forces, shear, bending or torsion (twisting).

The cylindrical bar in Figure 2-1 with an initial gage length, L_o, is subjected to an axial tensile load, P. The external load, P, is balanced by an internal resisting force

$$P = \int \sigma da$$

where σ is the stress normal to the end plane of the cylinder. If the stress is uniformly distributed, making σ a constant

$$\underline{\text{stress}} = \sigma = \frac{P}{A}$$

The stress causes an increase in length, $L_o + \delta$, and a slight decrease in diameter.

The linear average strain is

$$\underline{\text{strain}} = e = \frac{\delta}{L_o} = e = \frac{L - L_o}{L_o}$$

Strain is dimensionless since both δ and L_o have units of length.

Up to a limiting load the bar will recover its original dimension when the load is removed. This deformation is <u>elastic</u> (behaviour).

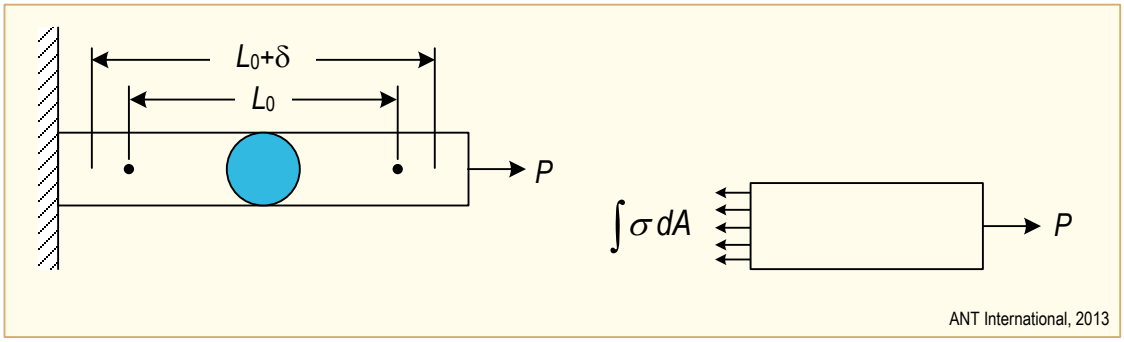

Figure 2-1: Cylindrical bar subjected to axial load.

Beyond the limiting load the bar will experience a permanent change in dimension. This deformation is <u>plastic</u> (behaviour).

Up to the limiting load the deformation is proportional to the load. In this case the average stress and strain are related by

Hooke's law: $\frac{\sigma}{e}$ = E = constant

where

E is the modulus of elasticity or Young's modulus (for zirconium alloys, the value of E is different in different directions; for example, 99 GPa (14×10^6 psi) in the a-crystallographic direction and 125 GPa (18×10^6 psi) in the c-direction at room temperature.

For elastic deformation, a stress in the longitude direction causes a positive strain in that direction and a negative strain in the perpendicular or transverse direction. The ratio of the strains in the two directions is called:

$$\text{Poisson's ratio} = \nu = \frac{transverse\ strain}{longitudinal\ strain}$$

The value of ν for metals is usually in the range of ν = 0.28 - 0.36 and for zirconium is taken as 0.33.

For Zircaloy tubing a similar parameter is sometimes used to express the ratio of axial strain to diametral strain when an axial stress is applied. This parameter combines both plastic and elastic strain, and is a variable depending on the crystallographic texture of the tubing and the amount of plastic strain applied.

$$\text{tubing contractile strain ratio} = \frac{diametral\ strain}{axial\ strain}$$

A standard engineering stress-strain curve is shown in Figure 2-2, with common terms for important parameters designated. A good description of stress-strain behaviour and terms given by Dowling [Dowling, 1999] is paraphrased below. (For our purposes the symbols for strain, ε and e, are both used to mean engineering strain, although a strict interpretation would usually result in ε being defined to mean true or instantaneous strain, ε = ln(1+e)).

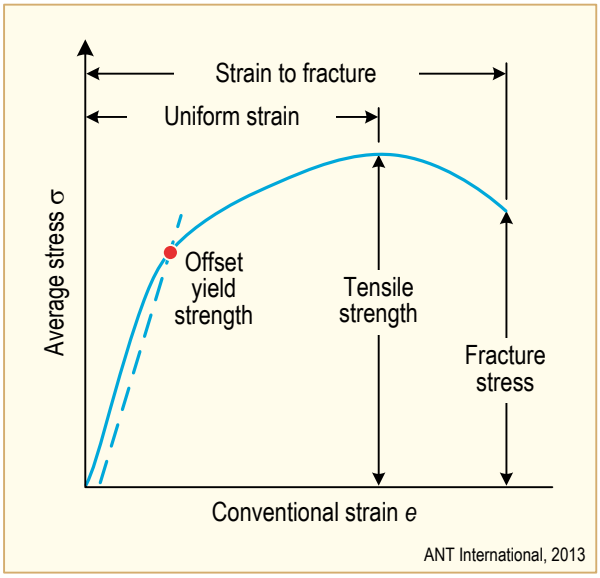

Figure 2-2: The engineering stress-strain curve.

The *ultimate tensile strength,* σ_μ, also called simply the *tensile strength*, is the highest engineering stress reached prior to fracture. If the behaviour is brittle, the highest stress occurs at the point of fracture. In ductile metals, the load, and hence the engineering stress, reaches a maximum and then decreases prior to fracture, as in Figure 2-2. In either case, the highest load reached at any point during the test, P_{max}, is used to obtain the ultimate tensile strength by dividing by the original cross-sectional area.

Eq. 2-1: $$\sigma_\mu = \frac{P_{max}}{A_1}$$

The *engineering fracture strength,* σ_f, is obtained from the load at fracture, P_f, even if this is not the highest load reached.

Eq. 2-2: $$\sigma_f = \frac{P_f}{A_1}$$

Hence, for brittle materials, $\sigma_\mu = \sigma_f$, whereas for ductile materials, σ_μ may exceed σ_f.

The departure from linear-elastic behaviour as in Figure 2-3 is called *yielding* and is of considerable interest because stresses that cause yielding, result in rapidly increasing deformation due to the contribution of plastic strain. Any strain in excess of the elastic strain σ/E is plastic strain and is not recovered on unloading. Hence, plastic strains result in permanent deformation. Such deformation in an engineering member changes its dimensions, or shape, or both, which is almost always undesirable. Thus, the first step in engineering design is usually to assure that stresses are sufficiently small that yielding does not occur, except perhaps in very small regions of a component.

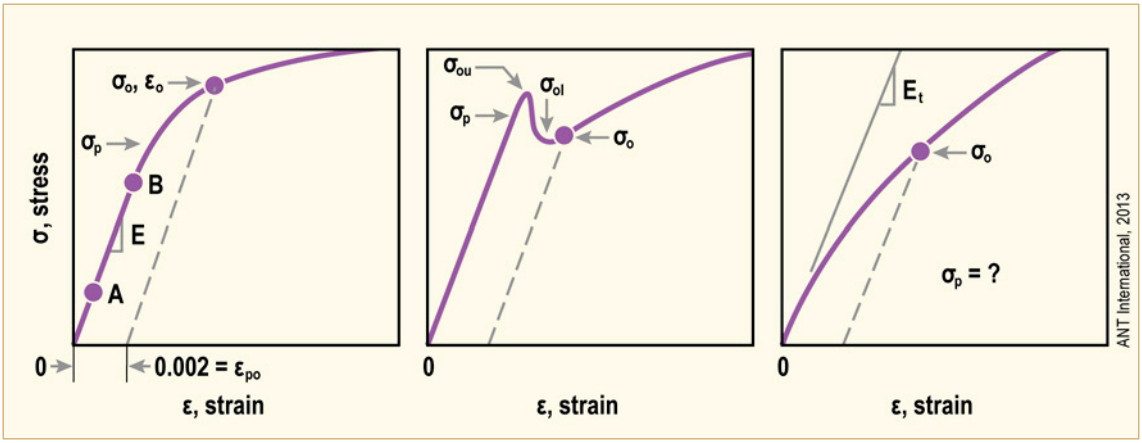

Figure 2-3: Initial portions of stress-strain curves: (a) many metals and alloys, (b) material with yield drop, and (c) material with no linear region, after [Dowling, 1999].

The yielding event can be characterized by several methods. The simplest is to identify the stress where the first departure from linearity occurs. This point is called the *proportional limit,* σ_ρ, and is illustrated in Figure 2-3. Some materials, as in (c), may exhibit a stress-strain curve with a gradually decreasing slope and no proportional limit. Even where there is a definite linear region, it is difficult to locate precisely where this ends. Hence, the value of the proportional limit depends on judgment, so is a poorly defined quantity. Another quantity sometimes defined is the *elastic limit*, which is the highest stress that does not cause permanent (i.e. plastic) deformation. Determination of this quantity is difficult, as periodic unloading to check for permanent deformation is necessary; its value also depends on the accuracy of the extensometer.

A third approach is the offset method, which is illustrated by dashed lines in Figure 2-3. A straight line is drawn parallel to the elastic slope, E or E_t, but offset by an arbitrary amount. The intersection of this line with the engineering stress-strain curve is a well-defined point that is not affected by judgment, except in cases where E_t is difficult to establish. This point is called the *offset yield strength,* σ_o. The most widely used and standardized offset for engineering metals such as Zircaloy is a strain of 0.002 that is 0.2%, although other values are also used. Note that the offset strain is a plastic strain, such as $\varepsilon_{po} = 0.002$, as unloading from σ_o would follow a dashed line in Figure 2-3, and this ε_{po} would be the unrecovered strain.

In some engineering metals, notably in low-carbon steels and often for irradiated Zircaloy, there is very little non-linearity prior to a dramatic drop in load as illustrated in Figure 2-3b. In such cases, one can identify an *upper yield point,* σ_{ou}, and a *lower yield point,* σ_{oi}. The former is the highest stress reached prior to the decrease, and the latter is the lowest stress prior to a subsequent increase. Values of the upper yield point in metals are sensitive to testing rate and to inadvertent small amounts of bending, so that reported values for a given material vary considerably. The lower yield point is generally similar to the 0.2% offset yield strength, with the latter having an advantage of being applicable to other types of stress-strain curves as well. The offset yield strength is generally the most satisfactory means of defining the yielding event for engineering metals.

Care has to be taken interpreting the strain at the maximum load. Calculation of the tensile behaviour of a perfectly cylindrical specimen shows that the load passes through a maximum value without the development of a neck. Necks form in real specimens, which are allowed by the ASTM standards, to have a central taper on cross-sectional area of up to 2%. These necks develop throughout the test but become noticeable only after the maximum load. Strictly, the attainment of a maximum load has little to do with the formation of a neck, although the elongation to maximum load is often called uniform strain. This behaviour is true for unirradiated materials and is even more pronounced for irradiated materials like Zircaloy, which is discussed later. Figure 2-4 illustrates the point for a typical ductile metal. In the elastic strain region and up to the ultimate tensile stress, the strain (in unirradiated material) is nearly uniformly distributed. Beyond this point (exceeding the uniform elongation (UE) or uniform strain) the strain tends to concentrate in a local area. The exact distribution will depend on the material, the amounts of cold work or irradiation, the gage length and the shape of the specimen cross-section. An illustration of non-uniform strain distribution is given in Figure 2-5 [Dieter, 1961]. More ductile materials have more deformation away from the necked region. Total elongation depends on specimen length because, although uniform elongation is independent of specimen length for unirradiated materials, necking localises deformation and is a higher proportion of a short specimen than a long specimen; using total elongation as the measure of ductility, a short specimen will appear more ductile than a long specimen. This effect is the reason that the specimen gage length must be reported along with the values of total strain.

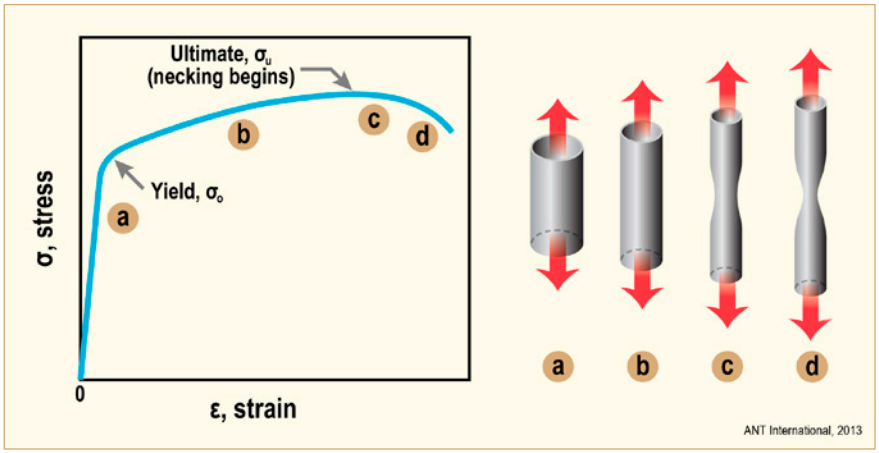

Figure 2-4: Schematic diagram of the engineering stress-strain curve of a typical ductile metal that exhibits necking behaviour, after [Dowling, 1999].

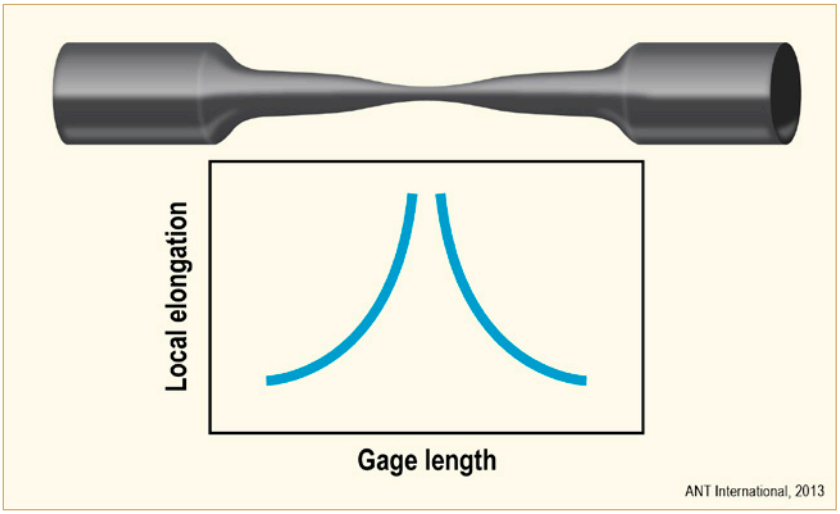

Figure 2-5: Schematic drawing of variation of local elongation with position along gage length of tensile specimen, after [Dieter, 1961].

Various standards exist for specimen dimensions. Generally the recommended ratio of gage length to width, or diameter, is 4 or 5. The width to thickness ratio can also affect the strain values [Chakrabarti & Spretnak, 1975]. With a constant gage length an increase in either width or thickness results in increased reported elongations. Ideally, the uniform elongation or strain should not be affected by specimen dimensions; however for irradiated material this is not the case, as discussed later.

An example of dimensions recommended by ASTM-E8M for one type of plate specimen is given in Figure 2-6.

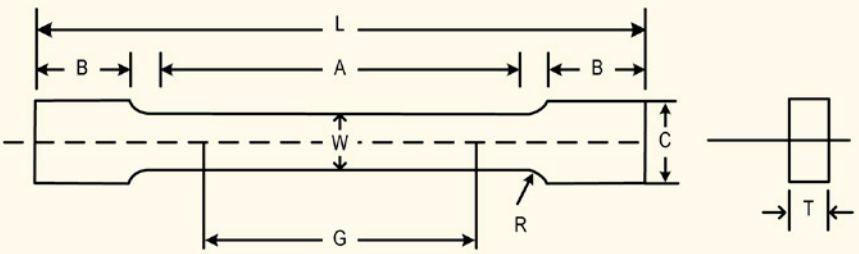

Dimensions, mm

Nominal width	Standard specimens		Subsize specimen
	Plate-type 40 mm	Sheet-type 12.5 mm	6 mm
G – Gage length	200.0 ± 0.2	50.0 ± 0.1	25.0 ± 0.1
W – Width	40.0 ± 2.0	12.5 ± 0.2	6.0 ± 0.1
T – Thickness		Thickness of material	
R – Radius of fillet, min	25	12.5	6
L – Overall length, min	450	200	100
A – Length of reduced section, min	225	57	32
B – Length of grip section, min	75	50	30
C – Width of grip section, approximate	50	20	10

ANT International, 2013

Figure 2-6: Rectangular tension test specimens.

It is clear that comparison of material ductility strain parameters is difficult if different test specimen geometries are used. A measure of ductility which is not so much affected by specimen geometry is reduction of area, RA. RA is quite sensitive to material microstructure and therefore is useful for zirconium alloy specimens. RA is defined

$$\% \text{ RA} = 100 \ \frac{A_i - A_f}{A_i}$$

where A_i is the initial cross-sectional area and A_f is the final cross-sectional area after fracture. RA is not easy to measure on highly irradiated material, but it can and should be done. The fracture cross-section of specimens starting with circular cross-section may become elliptical, providing an indication of crystallographic texture. $A_f = \pi ab$, where a and b are the semi-axes of the ellipse.

In standard specifications, total elongation on a gauge length of 50 mm is the usual measure of ductility; at room temperature and 300°C (573 K) tubes made from recrystallized Zircaloy and Zr2.5Nb must have an elongation ≥20% while those made from cold-worked and stress-relieved Zr2.5Nb must have an elongation ≥ 12% [Anonymous, 2007a and b]. Reduction in area is not a requirement and neither is some evaluation of work-hardening nor strain-rate hardening.

It is sometimes useful to compare materials or material conditions by the strain hardening ratio, SHR

$$\text{SHR} = \frac{\sigma_u}{\sigma_o}$$

where σ_u is the ultimate tensile stress and σ_o (or σ_y) is the yield stress. Values >1.4 are considered high for metals, while values <1.2 are low [Dowling, 1999]. By those criteria, unirradiated Zircaloy is in the "high" range, with the exact values depending on strain rate, stress state and texture.

Another concept encountered in analysing tensile test is true stress and true strain. For a ductile material, the cross-sectional area is continually getting smaller as strain increases, so use of the original area gives an underestimate of the actual instantaneous stress. Comparison of an engineering and true stress-strain curve is given in Figure 2-7 [Dieter, 1961]. True strain is defined as the summation of strains over small increments, i.e.

$$\tilde{\varepsilon} = \int_{L_i}^{L} \frac{dL}{L} = \ln \frac{L}{L_i}$$

where L is the instantaneous length, $L_i + \Delta L$.

Therefore: $$\tilde{\varepsilon} = \ln(1+e)$$

where e is the engineering strain, $\frac{\Delta L}{L}$.

Using the fact that plastic strain is essentially a constant volume process,

$$A_i L_i = AL$$

and

$$\frac{A_i}{A} = \frac{L}{L_i} = \frac{L_i + \Delta L}{L_i} = 1 + e$$

Since true stress, $\tilde{\sigma} = \sigma\left(\frac{A_i}{A}\right)$

then $\tilde{\sigma} = \sigma(1+e)$.

These equations strictly apply only beyond the elastic range (volume is not constant in the elastic range) and below the point of uniform elongation, but they often are used over the whole stress-strain range. If experimental measurements of the cross-section are available, the true stress can be plotted directly. And some analytical corrections are available to account for necking. The true stress-strain curve is sometimes called the flow curve, and is used in design and performance analyses.

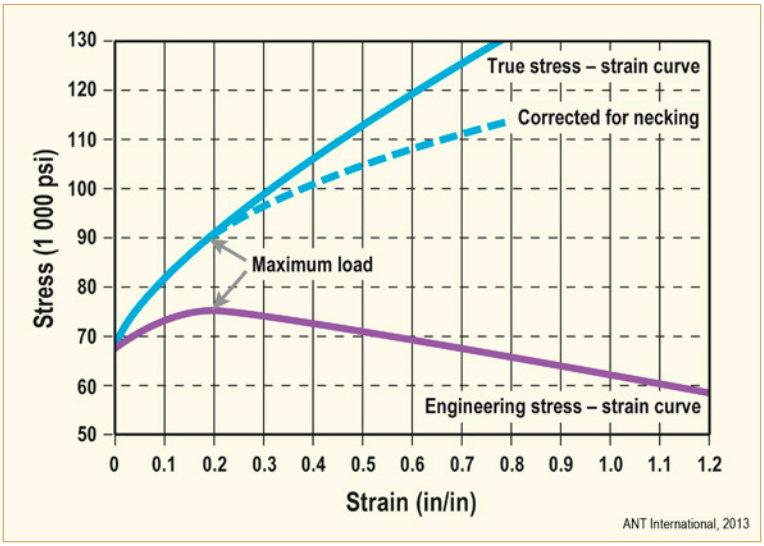

Figure 2-7: Comparison of engineering and true stress-strain curves for a ductile metal, after [Dieter, 1961].

2.1.2 Stress and strain in multiaxial loading (Ron Adamson and Peter Rudling)

2.1.2.1 Introduction

In practice, the distribution of stress and strain in a component is complex. Figure 2-8 shows the six components of stress that are needed to describe the state of stress at a point. Those stresses acting normal to a surface are designated as normal stresses σ and those that act parallel to the surfaces are the shear stresses τ.

3 Tensile testing (Ron Adamson)

3.1 Introduction

Tensile properties of zirconium alloy components is essential to understanding reactor component behaviour and to insure safe reactor operation. Although due to the nature of test data needed (unique component geometry and radioactivity of the materials,) many test techniques used in the Industry are not "standard", several ASTM International Standard Practice documents are useful and applicable:

- E8/E8M- Test methods for Tension Testing of Metallic Materials
- E83- Practice for Verification and Classification of Extensometer Systems
- E21- Standard Tests Methods of Elevated Temperature Tension Tests of Metallic Materials
- E6- Standard Terminology Relating to Methods of Mechanical Testing

Section 2 describes in detail the normal ways to plot and use stress and strain, and the meaning of various mechanical metallurgy concepts.

3.2 Testing apparatus

Although coming in many forms, the workhorse tensile test machine is the closed-loop servo-hydraulic system shown schematically in Figure 3-1. Older systems, not shown, are mechanically driven by heavy-duty screws, while the illustrated system uses an oil-pressurized piston. The screwdriver machines have the advantage of providing a controllable and steady motion, while the servo-hydraulic machines are able to provide variations in load or movement patterns.

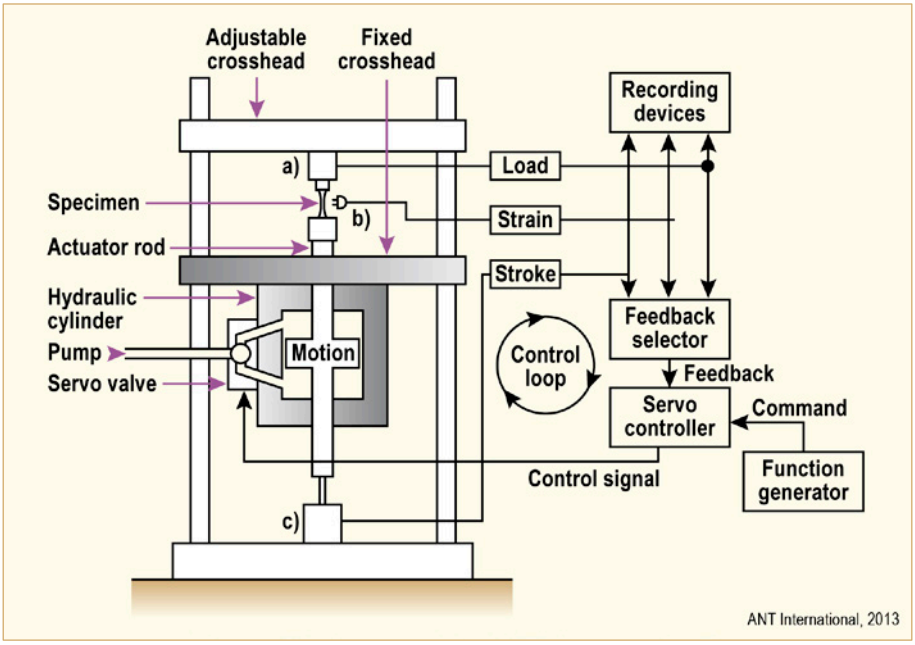

Figure 3-1: Modern closed-loop servo-hydraulic testing system, schematic diagram, after [Dowling, 1999].

Three sensors are employed: (a) load cell, (b) extensometer, and (c) LVDT.

Applied force or load is measured by a load cell and elongation of the specimen is obtained either by an extensometer attached or focused on the specimen gage or by electronically monitoring the motion of the machine cross-head. In the latter case, the moving parts of the loading system must be rigid or stiff to insure all measured motion can be attributed to the specimen. In the former case, extensometers include LVDTs (linear variable differential transformers), strain gauges, and non-contact laser devices.

The test specimen is attached to the loading/strain system by some form of grips. ASTM Standard E8/E8M recommends standard grips, but often special grips must be designed to fit the specimen design, to be discussed later. Grips and load-bearing components are made of high strength-creep resistant alloys such as 17-4PH stainless steel, MarM247C [Alam & Hellwig, 2009] or in case of PCl/SCC-environment testing, a molybdenum alloy [Coffin, 1979].

Strain rate on the specimen during the test can be important. Normally strain rates are in the range $3x10^{-5}$ s^{-1} (slow) to $1x10^{-3}$ s^{-1} (fast). For reference, to obtain 5% strain at a rate of $5x10^{-4}$ s^{-1} would take about 100 seconds.

Under normal conditions reactor zirconium alloy components operate in the broad temperature range 270°C (543K) to 375°C (648K). During shutdowns or handling in the storage pool the temperatures approach but are generally above "room" temperature, loosely defined here as 30°C (303K). This entire range of specimen temperatures can be easily attained by heating systems, including clam-shell incandescent heaters, by induction coils around the specimen or by electrical resistance heating through the specimen. Since testing times are short, testing in air is normally satisfactory.

Temperature control is usually accomplished by thermocouples attached to the specimen or grips, or in rare cases by infrared temperature monitors.

Radiation-damage annealing in zirconium alloys begins at about 350°C (623K) and becomes rapid at 400°C (673K). For a recent review see Section 5 of ZIRAT17/IZNA12 Annual Report [Rudling et al, 2012].

3.3 Material source

The source of material and specimens for testing is generally the reactor components themselves, e.g., tubing and flat products of various sizes. Table 3-1 gives a sample of dimensions for typical components. It is seen that for BWRs and PWRs, dimensions are small and often are not suitable for fabricating standard specimen geometries. The same is true for CANDU components, although pressure tube dimensions are significantly larger than fuel cladding.

4 Hardness testing (Tahir Mahmood)

Hardness of a metal is a measure of how resistant the metal is to various kinds of permanent shape change when a force is applied. The key to understanding the mechanism behind hardness is understanding the metallic microstructure, or the structure and arrangement of the atoms at the atomic level. In fact, most important metallic properties critical to the manufacturing of today's components are determined by the microstructure of a material. At the atomic level, the atoms in a metal are arranged in an orderly three-dimensional array called a crystal lattice. In reality, however, a given specimen of a metal likely never contains a consistent single crystal lattice. A given sample of metal will contain many grains, with each grain having a fairly consistent array pattern. At an even smaller scale, each grain contains irregularities.

There are two types of irregularities at the grain level of the microstructure that are responsible for the hardness of the material. These irregularities are point defects and line defects. A point defect is an irregularity located at a single lattice site inside of the overall three-dimensional lattice of the grain. There are three main point defects. If there is an atom missing from the array, a vacancy defect is formed. If there is a different type of atom at the lattice site that should normally be occupied by a metal atom, a substitutional defect is formed. If there exists an atom in a site where there should normally not be, an interstitial defect is formed. This is possible because space exists between atoms in a crystal lattice. While point defects are irregularities at a single site in the crystal lattice, line defects are irregularities on a plane of atoms. Dislocations are a type of line defect involving the misalignment of these planes. In the case of an edge dislocation, a half plane of atoms is wedged between two planes of atoms. In the case of a screw dislocation two planes of atoms are offset with a helical array running between them.

Dislocations provide a mechanism for planes of atoms to move past one another and thus provide a method for plastic or permanent deformation. Planes of atoms can flip from one side of the dislocation to the other effectively allowing the dislocation to traverse through the material and the material to deform permanently. The movement allowed by these dislocations causes a decrease in the material's hardness.

The way to inhibit the movement of planes of atoms, and thus make them harder, involves the interaction of dislocations with each other and interstitial atoms. When a dislocation intersects with a second dislocation, it can no longer traverse through the crystal lattice. The intersection of dislocations creates an anchor point and does not allow the planes of atoms to continue to slip over one another. A dislocation can also be anchored by the interaction with interstitial atoms. If a dislocation comes in contact with two or more interstitial atoms, the slip of the planes will again be disrupted. The interstitial atoms create anchor points, or pinning points, in the same manner as intersecting dislocations.

By varying the presence of interstitial atoms and the density of dislocations, a particular metal's hardness can be controlled. Although seemingly counter-intuitive, as the density of dislocations increases, there are more intersections created and consequently more anchor points. Similarly, as more interstitial atoms are added, more pinning points that impede the movements of dislocations are formed. As a result, the more anchor points added, the harder the material will become. In irradiated Zircaloys, the irradiation-induced <a> loops act as barriers to dislocation motion. More details are available in Chapter 2 of the ZIRAT14/IZNA9 STR "In-Reactor Creep of Zirconium Alloys" and Section 4 of the ZIRAT15/IZNA10 AR.

4.1 Hardness measurement techniques

Hardness of a material is a rather ill-defined term. It is related to strength and ductility, to resistance to plastic deformation, to wear resistance; however, it is most commonly defined as resistance to indentation. All of the hardness tests evaluate indentations in one way or another. Hardness measurement can be defined as macro-, micro- or nano- scale according to the forces applied and displacements obtained. Measurement of the macro-hardness of materials is a quick and simple method (compared to tensile and creep testing etc., and only if done correctly) of obtaining mechanical property data for the bulk material from a small sample. It is also widely used for the quality control of surface treatment processes. However, when concerned with coatings and surface properties of importance to friction and wear processes for instance, the macro-indentation depth would be too large relative to the surface-scale features.

Where materials have a fine microstructure, are multi-phase, non-homogeneous, or prone to cracking, macro-hardness measurements will be highly variable and will not identify individual surface features. It is here that micro-hardness measurements are appropriate. Micro-hardness is the hardness of a material as determined by forcing an indenter such as a Vickers or Knoop indenter into the surface of the material under 15 to 1000 gf load; usually, the indentations are so small that they must be measured with a microscope. The technique is capable of determining hardness of different micro-constituents within a structure, or measuring steep hardness gradients such as those along the wall thickness of unirradiated and irradiated Zircaloy cladding. Conversions from micro-hardness values to tensile strength and other hardness scales (e.g. Rockwell) are available for many metals and alloys [ASTM E140, 2013].

Nano-indentation tests measure hardness by using very small, on the order of 1 nano-Newton, indentation forces and measuring the depth of the indention that was made. These tests are based on new technology that allows precise measurement and control of the indenting forces and precise measurement of the indentation depths. By measuring the depth of the indentation, progressive levels of force are measurable on the same piece. This allows the tester to determine the maximum indentation load that is possible before the hardness is compromised. This also allows a check to be completed to determine if the hardness remains constant even after an indentation has been made.

The multiplicity of definitions, and corresponding multiplicity of hardness measuring instruments, together with the lack of a fundamental definition, indicates that hardness may not be a fundamental property of a material, but rather a composite one including yield strength, work hardening, true tensile strength, modulus of elasticity, and others. A variety of tests are commonly used. The most useful are discussed here. They each use an indenter of a unique shape and a hardness number is calculated using the amount of deformation which is produced by a given applied load on the indenter. They all require careful surface preparation if the data is to be reproducible and of high quality. The “macro-tests” are most robust and useful for less-than-ideal conditions; the “micro-tests” require strict attention to specimen preparation details (e.g., specimen flatness, smoothness, uniformity). The following types of hardness tests are generally used by the industry

1) Rockwell hardness
2) Brinell hardness
3) Vickers hardness
4) Knoop hardness

The way these hardness tests measure a metal's hardness is to determine the metal's resistance to the penetration of a non-deformable ball or cone. The tests determine the depth which such a ball or cone will sink into the metal, under a given load, within a specific period of time. Although elevated-temperature (hot) hardness techniques and equipment are available, they are not often used and these tests are carried out at an ambient temperature within the limits of 10 to 35°C [ASTM E10, E18, E384, 2013].

5 Burst testing (Kit Coleman)

During reactor operation various tubes are internally stressed:

1) Fuel cladding must withstand fuel expansion and resist internal pressurisation from a filler gas and build up of fission gasses;

2) In a reactor that uses tubes as its pressure vessel, for example, CANDU and RBMK, the water has to be pressurized up to about 11 MPa to maintain the heat-transport water as a liquid at about 300°C.

3) If a pressure tube should fail in CANDU, it would be desirable if the tube surrounding it, called a calandria tube, survived being pressurised.

When tubes are stressed in tension they may yield and eventually rupture. The values of the mechanical response, yield strength, ultimate strength and ductility (usually based on change of diameter) can be measured in biaxial tests with various ratios of hoop to axial stress. The most common test mode is the closed-end burst test in which the ratio of hoop to axial stress is 2:1. It is used to show that components meet a specification, how they respond to reactor operation - especially neutron irradiation, the degree of texture strengthening and the resistance of the material to crack growth.

5.1 Closed-end pressurisation

5.1.1 Fuel cladding

In 1970 ASTM decided that a standard method for evaluating the mechanical response of fuel cladding to internal pressure was needed. A round-robin exercise between four laboratories was used with tests at room temperature to compare the various methods available at the time. The machines and results were described at the Second Zirconium Symposium by [Hardy et al, 1974] and the method is included as an option in ASTM Standards B 353-12 and B 811-13 [Anonymous, 2012, 2013]. These standards only mention tests at room temperature but allow for tests at elevated temperatures so long as appropriate stable fluids are used as the pressurising medium. A typical apparatus is depicted in Figure 5-1 [Hardy, 1970]. The criteria for a successful test are:

1) The system should have adequate capacity to accommodate the anticipated pressure.

2) The pressure should increase at a steady rate without surges; in the elastic region this rate should be 13.8±1.4 MPa/min. The pumping rate should be maintained for the duration of the test up to burst. All air should be purged from the system to reduce stored energy and provide stiffness.

3) Gauges with adequate capacity should be used to follow the system pressure, P.

4) To minimise end-effects, the minimum length of a specimen should be $10D_O$, where D_O is the outside diameter of the cladding. The end fixtures should allow relative axial movement so the ratio of hoop to axial stress is 2:1.

5) A mandrel may be used to minimise volume inside the specimen and maintain straightness. The mandrel outside diameter, D_M, should be 0.25±0.05 mm less than the inside diameter of the cladding, D_I. The original recommendation for clearance in [Hardy et al, 1974] was larger – $D_I/(D_I-D_M)$ of 20 – and with a typical cladding (D_O of 9.5 mm and wall thickness, t, of 0.7 mm), the clearance would be 0.4 mm. The ends of the mandrel should not restrict axial deformation.

6) The hoop stress, σ_H, is calculated from:

Eq. 5-1: $$\sigma_H = PD_I/2t$$

7) The total circumferential elongation (%TCE) is estimated at the point of maximum bulge, excluding the opening at rupture. The final circumference, C_F, is usually measure by flexible tape.

Eq. 5-2: $$\%TCE = (C_F - \pi D_O)/ \pi D_O$$

8) For tests at room temperature, water is an acceptable pressurising fluid. At elevated temperatures the pressurising fluid should be stable; for example, a silicone oil.

9) The specified minimum Ultimate Hoop Strength is 500 MPa and TCE is 20% for recrystallized Zircaloy at room temperature.

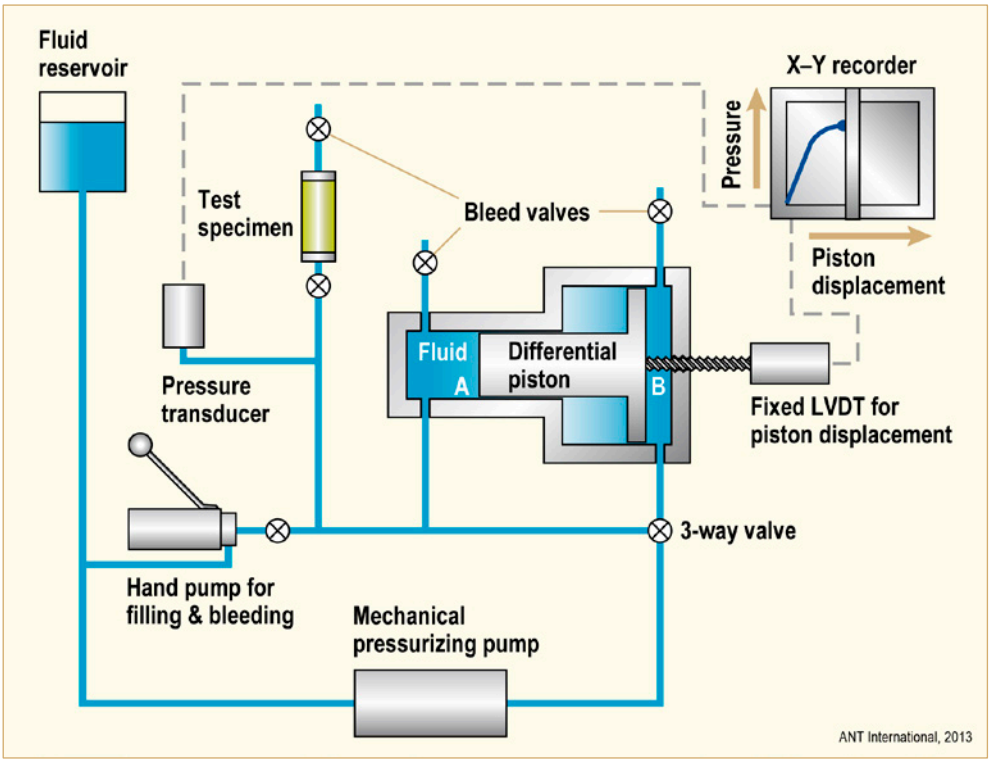

Figure 5-1: Apparatus for closed-end burst-testing fuel cladding, after [Hardy, 1970].

Other countries followed a similar approach. For example, in Japan [Mishima, 1977] the specimen was 150 mm long (about $16D_0$) and the clearance between the mandrel and inside of tube was 0.5 mm.

In the 21st century the basic apparatus has not changed, except that specimen dimensions may be measured directly during the test, rather than relying on change in volume, and the data are collected and analysed by computer rather than X-Y recorder.

6 Creep testing (Ron Adamson)

6.1 Introduction

Creep is defined as a time dependent change in dimension of a reactor component (or any material) under a stress. Creep is plastic deformation occurring as a constant volume process, normally at low stresses below the yield stress. **For materials in an irradiation field, the most important for purposes of this Section of the AR being the neutron environment of a nuclear reactor,** the deformation occurs by the motion of dislocations and irradiation-produced defects under the influence of stress. Neutron irradiation produces large quantities of point defects – vacancies and SIAs (self-interstitial atoms) – which migrate to and collect at various sinks. Due to the anisotropy of the zirconium crystal lattice, motion of both dislocations and SIAs is anisotropic, preferring to occur parallel to the basal plane in the <a> directions of the lattice. Dislocations are sinks for both vacancies and SIAs, but normally it is considered that an edge dislocation attracts SIAs more than vacancies. Dislocations produced by deformation and by irradiation lie on both basal and prism planes. Because of the diffusional anisotropy of SIAs, they tend to be absorbed by dislocations lying on prism planes. The diffusion of vacancies is isotropic, and they tend to be absorbed preferentially by dislocations lying on basal planes. Similarly, SIAs tend to be absorbed at grain boundaries oriented parallel to prism planes and vacancies on boundaries parallel to basal planes. Absorption of either vacancies or SIAs at dislocations of grain boundaries causes plastic strain; positive for SIAs and negative for vacancies. If the absorptions occurred randomly and in non-biased fashion, the net strain would be zero; however in zirconium alloys the built-in anisotropy results in separate positive and negative strains, and in constant volume deformation. Also, in addition to the natural anisotropy of the zirconium crystal lattice, an important factor is the concept that anisotropic diffusion is enhanced by stress.

Many mechanisms of irradiation creep have been proposed, as discussed in detail by [Adamson et al, 2009] and [Holt, 2008]. No single mechanism has been accepted as the dominating mechanism, and very likely several processes contribute simultaneously. The two most prominent mechanisms are SIPA (Stress Induced Preferential Absorption) and climb and glide. SIPA assumes a bias of the motion of vacancies and SIAs to dislocations depending on the orientation of the Burgers vectors with respect to the applied shear stress. There are several variations of SIPA, including the elasto-diffusion modification which invokes the effect of stress on the diffusion anisotropy itself. Elasto-diffusion appears to have the strongest effect on creep within the SIPA "family".

The most straightforward irradiation creep mechanism is the climb and glide mechanism, by which deformation-producing dislocations are aided in bypassing obstacles to their motion by irradiation produced point defects (Figure 6-1). As long as an individual dislocation attracts a net flux of either vacancies or SIAs, it can "climb around" a barrier and under the influence of an applied stress, glide to the next barrier, thereby producing strain and eventually cause a slip step at the material surface. The weak dependence of creep rate on dislocation density suggests that glide may not be the main strain-generating process.

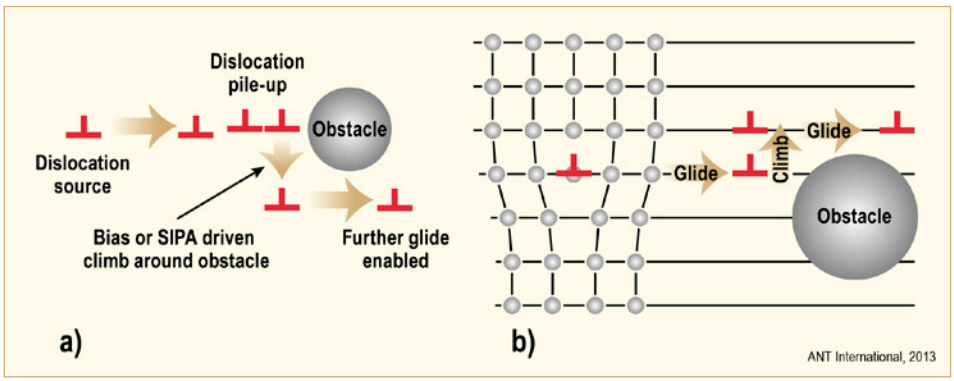

Figure 6-1: Schematic diagram of climb and glide process, after a) [Matthews & Finnis, 1988] and b) [Dowling, 1999].

A further contributor to the strain measured in a creep experiment is irradiation growth. Although not strictly in the "creep" category because it occurs in the absence of an applied stress, it is inevitably measured as part of the overall strain in all in-reactor experiments. Irradiation growth results from mechanisms similar to irradiation creep in that it is dependent on the anisotropic properties of the zirconium crystal lattice, see Section 2.3 and [Adamson et al, 2009].

Creep experiments in a neutron-irradiation environment have been conducted since the early 1960's, and continue today. Since creep without irradiation tends to have a relatively high initial rate, and since irradiation damage builds up with time, the creep curve (strain versus time or fluence) is usually divided into primary and a secondary stages, as shown in Figure 6-2. High burnup implies long times, but for in-reactor service the third stage (tertiary or unstable) creep is rarely reached. Generally the secondary (steady state) creep stage is approached (Figure 6-3).

Whether or not true time "steady state" creep rate is obtained in-reactor is problematic, but in many cases it is assumed for the analysis of the important parameters. A tertiary stage is not reached except in very rare localized high stress cases.

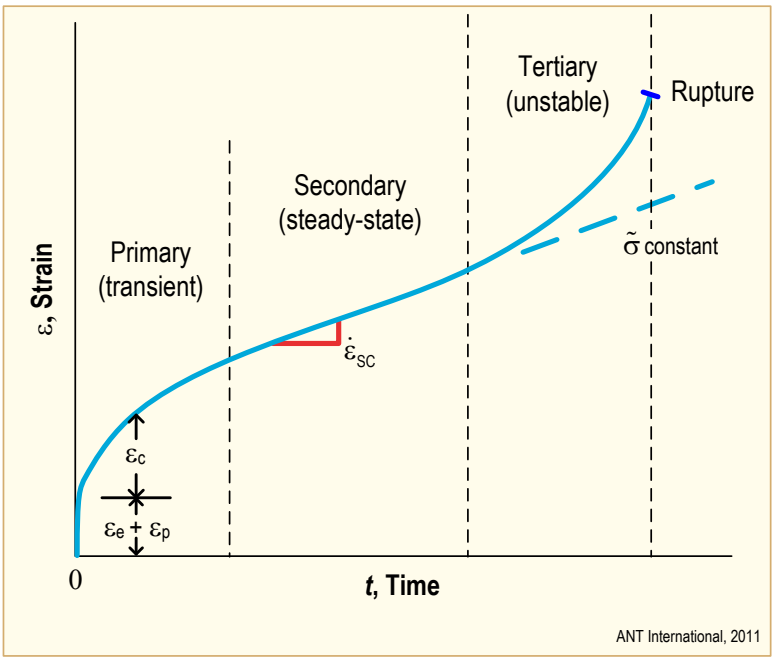

Figure 6-2: Idealized strain vs. time behaviour during creep under constant load, and the three stages of creep.

7 Fatigue and fatigue crack propagation testing (Tahir Mahmood and Ron Adamson)

7.1 Introduction

In materials science, fatigue is the progressive and localized structural damage that occurs when a material is subjected to cyclic loading. The nominal maximum stress values are less than the ultimate tensile stress limit, and may be below the yield stress limit of the material. Fatigue occurs when a material is subjected to repeated loading and unloading. If the loads are above a certain threshold, microscopic cracks begin to form at the stress concentrators such as the surface, persistent slip bands, and grain interfaces [Kim & Laird, 1978]. Eventually a crack reaches a critical size, and the structure suddenly fractures. The shape of the structure significantly affects the fatigue life; square holes or sharp corners lead to elevated local stresses where fatigue cracks can initiate. Round holes and smooth transitions or fillets are therefore important to increase the fatigue strength of the structure.

ASTM defines fatigue life, N_f, as the number of stress cycles of a specified character that a specimen sustains before failure of a specified nature occurs [Stephens & Fuchs, 2001]. One method to predict fatigue life of materials is the Uniform Material Law (UML) [Bäumel & Seeger, 1990]. UML was developed for fatigue life prediction of aluminium and titanium alloys by the end of 20th century and extended to high-strength steels [Korkmaz, 2010] and cast iron [Korkmaz, 2011]. For some materials, there is a theoretical value for stress amplitude below which the material will not fail for any number of cycles, called a fatigue limit, endurance limit, or fatigue strength [Bathias, 1999]. Various fatigue characteristics of metal alloys include the following.

- In metal alloys, when there are no macroscopic or microscopic discontinuities, the process starts with dislocation movements, eventually forming persistent slip bands that nucleate short cracks.
- Macroscopic and microscopic discontinuities as well as component design features which cause stress concentration (keyways, sharp changes of direction etc.) are the preferred location for starting the fatigue process.
- Fatigue is a stochastic process, often showing considerable scatter even in controlled environments.
- Fatigue is usually associated with tensile stresses but fatigue cracks have been reported due to compressive loads [Fleck et al, 1985].
- The greater the applied stress range, the shorter the life.
- Fatigue life scatter tends to increase for longer fatigue lives.
- Damage is cumulative. Materials do not recover when rested.
- Fatigue life is influenced by a variety of factors, such as temperature, surface finish, microstructure, presence of oxidizing or inert chemicals, residual stresses, contact (fretting), etc.
- Some materials (e.g., some steel and titanium alloys) exhibit a theoretical fatigue limit below which continued loading does not lead to structural failure.
- High cycle fatigue strength (about 10^3 to 10^8 cycles) can be described by stress-based parameters. A load-controlled servo-hydraulic test rig is commonly used in these tests, with frequencies of around 20–50 Hz. Other sorts of machines—like resonant magnetic machines—can also be used, achieving frequencies up to 250 Hz.
- Low cycle fatigue (typically less than 10^3 cycles) is associated with widespread plasticity in metals; thus, a strain-based parameter should be used for fatigue life prediction in metals and alloys. Testing is conducted with constant strain amplitudes typically at 0.01–5 Hz.

The factors that affect fatigue life of a component include:

- **Cyclic stress state**: Depending on the complexity of the geometry and the loading, one or more properties of the stress state need to be considered, such as stress amplitude, mean stress, biaxiality, in-phase or out-of-phase shear stress, and load sequence.

- **Geometry**: Notches and variation in cross-section throughout a part lead to stress concentrations where fatigue cracks initiate.

- **Surface quality**: Surface roughness cause microscopic stress concentrations that lower the fatigue strength. Compressive residual stresses can be introduced in the surface by e.g. shot peening to increase fatigue life. Such techniques for producing surface stress are often referred to as peening, whatever the mechanism used to produce the stress. Low plasticity burnishing, laser peening, and ultrasonic impact treatment can also produce this surface compressive stress and can increase the fatigue life of the component. This improvement is normally observed only for high-cycle fatigue.

- **Material Type**: Fatigue life, as well as the behaviour during cyclic loading, varies widely for different materials, e.g. composites and polymers differ markedly from metals.

- **Residual stresses**: Welding, cutting, casting, and other manufacturing processes involving heat or deformation can produce high levels of tensile residual stress, which decreases the fatigue strength.

- **Size and distribution of internal defects**: Casting defects such as gas porosity, non-metallic inclusions and shrinkage voids can significantly reduce fatigue strength.

- **Air or Vacuum**: Certain materials like Metals are more prone to fatigue in air than in a vacuum. Depending upon the level of humidity and temperature, the lifetime for metals such as aluminium or iron might be as much as 5 to 10 times greater. This is mostly due to the effect of the oxygen and water vapour in the air which will aggressively attack the material and so encourage the propagation of cracks. Other environments such as oil or seawater may perform better than air but they will also be worse than a vacuum [Milella, 2013].

- **Direction of loading**: For anisotropic materials, like Zircaloys, fatigue strength depends on the direction of the principal stress.

- **Grain size**: For most metals, smaller grains yield longer fatigue lives, however, the presence of surface defects or scratches will have a greater influence than in a coarse grained alloy. [Sanders & Starke, 1977] have determined that refinement of grains improved the low cycle fatigue of zirconium alloys though improved homogeneity of deformation which delayed crack initiation and failure.

- **Environment**: Environmental conditions can cause erosion, corrosion, or gas-phase embrittlement, which all affect fatigue life. Corrosion fatigue is a problem encountered in many aggressive environments.

- **Temperature**: Extreme high or low temperatures can decrease fatigue strength.

- **Crack Closure**: Crack closure is a phenomenon in fatigue loading, during which the crack will tend to remain in a closed position even though some external tensile force is acting on the material. During this process the crack will open only at stress above a particular crack opening stress. This is due to several factors such as plastic deformation or phase transformation during crack propagation, corrosion of crack surfaces, presence of fluids in crack, or roughness at cracked surfaces etc. this will provide a longer fatigue life for the material than expected, by slowing the crack growth rate.

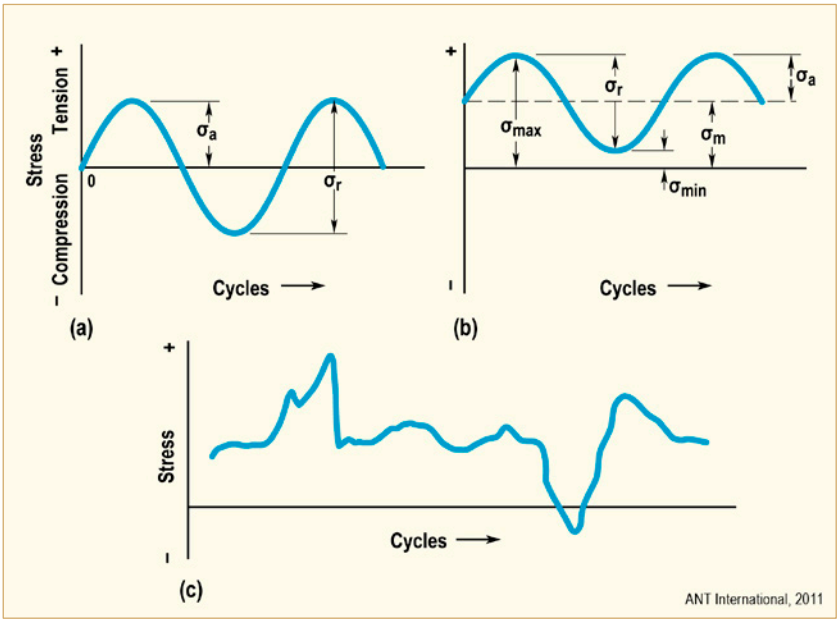

Figure 7-1: Typical fatigue stress cycles. (a) Reversed stress; (b) repeated stress; (c) irregular or random stress cycle, after [Dieter, 1961].

The stress ratio, R, is defined as the ratio of the minimum to maximum loads, $\sigma_{min}/\sigma_{max}$. Several types of loading are illustrated by static loading, R = 1; tensile cycle loading, 0<R<1; reversed load cycling, -1<R<0; symmetrical load cycling, R = -1.

Figure 7-1c illustrates a complicated stress cycle, which could be induced, for instance, in a component by thermo-hydraulic-induced vibrations. Some useful terms for these cases are included in Table 7-1.

Table 7-1: Useful terms relating to fatigue.

S, as in S-N curve	Stress
stress range,	$\Delta a = \sigma_{max} - \sigma_{min}$
mean stress,	$\sigma_m = (\sigma_{max} + \sigma_{min})/2$
stress amplitude	$\sigma_a = \Delta\sigma/2$
alternating stress	$\sigma_a = \Delta\sigma/2$
stress ratio	$R = \sigma_{min}/\sigma_{max}$
fatigue (endurance) limit	E_l = stress below which fatigue failure does not normally occur
fatigue strength	= stress amplitude value from S-N curve at a particular life of interest
high cycle fatigue	= when fatigue life is greater than about 10^6 cycles
Low Cycle Fatigue (LCF)	= when fatigue life is below about 10^5 cycles
strain amplitude	$\varepsilon_a = \frac{\Delta\varepsilon}{2}$
number of cycles to failure	= N_f
plastic strain	= $\Delta\varepsilon_p$ = width of hysteresis loop
plastic strain amplitude, E_{ap}	= $\Delta\varepsilon_p/2$
	ANT International, 2011

8 Fracture toughness testing (Ron Adamson)

8.1 Introduction

In practice all engineering components can have defects in the form of small cracks that form during fabrication or as they are used in service. The questions that arise are "how easily will the crack propagate?" and "will the crack compromise safe operation of the component?" To provide answers to such generic questions, the technology and science of *fracture mechanics* was developed. Extensive employment of fracture mechanics to cracking issues in steels and other high strength alloys has resulted in increased safety in pressure vessels, aircraft engines, building structures and many other commercial and military applications. A very useful review of the early literature of fracture mechanics is provided by [Barsom, 1987]. Early extension into the field of non-ductile fracture was facilitated by [Rice, 1968], [Sih, 1989] and others.

Use of fracture mechanics technology for reactor zirconium alloy issues has been limited in the past. This is partly due to a lack of regulatory emphasis on cladding failure as a safety issue and to the fact that, as explained below, much of the standard fracture mechanics methodology does not apply to reactor bundle component geometry. The use of fracture mechanics to predict the behaviour of cracks or defects in cladding is increasing because the probability of operation with defects present increases with burnup and as new zirconium alloys are introduced. Papers at recent international conferences have illustrated fracture mechanics techniques for analysing crack propagation in failed Zircaloy fuel cladding, for example [Yagnik et al, 2009]. And for many years, a leak-before-break criterion and critical crack lengths in CANDU-type pressure tubes have been analysed, with considerable success, using fracture toughness methodology [Simpson & Chow, 1987], [Chow & Simpson, 1988], [Simpson et al, 1989].

A small crack in a large member can substantially alter the stress distribution and magnitude near the crack. At the edge of a crack, parallel to an applied tensile stress, the tensile stress is many times higher than the nominal applied stress, as illustrated in Figure 8-1 [Dowling, 1999]. For an elastic material as the radius of the crack tip approaches zero, the stress there would approach infinity.

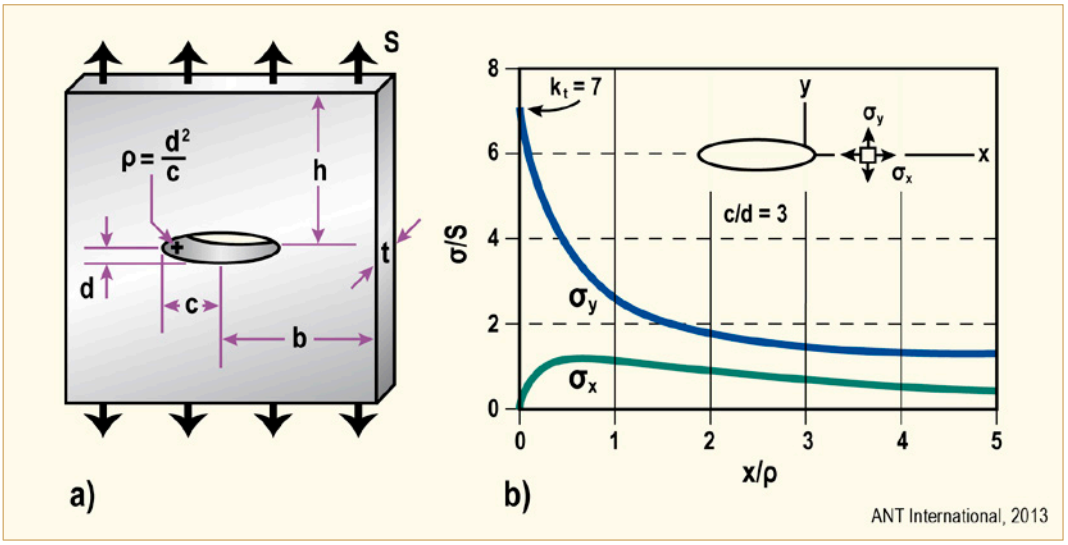

Figure 8-1: Elliptical hole in a wide plate under remote uniform tension and the stress distribution along the x-axis near the hole for one particular case, after [Dowling, 1999].

In a ductile material like Zircaloy, the stress at the crack tip is relieved by plastic deformation, so the local stress does not go to infinity, but peaks at about 2-3 times the applied stress. The effects of irradiation and dislocation channelling on crack tip deformation are not well understood. A plastic zone develops (Figure 8-2), in which the stresses are strongly influenced by the crack tip. If the size of the plastic zone is not "too large" (to be quantified later), the theory of linear-elastic fracture mechanics (LEFM) can be used to determine what combination of crack size, crack and component geometry, and applied tensile stress will result in component operation without danger of rapid crack propagation.

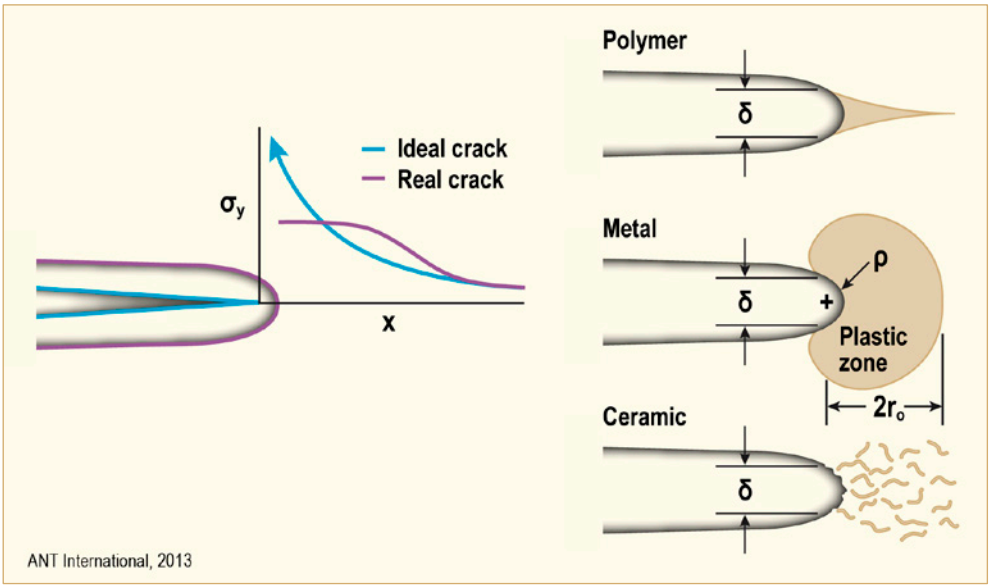

Figure 8-2: Finite stresses and nonzero radii at tips of cracks in real materials. A region of intense deformation forms due to plasticity, crazing, or microcracking, after [Dowling, 1999].

A basic feature of LEFM is the stress intensity factor, K, which is a function of the applied stress, S, the crack length, a, and a crack and specimen geometry factor, g.

For example a relation like

Eq. 8-1: $$K = S(\pi a)^{0.5}$$

applies to a simple wide plate with a well-defined crack at its centre.

In tension, when the value of K is below a critical value, K_{Ic}, a given material can resist rapid crack propagation or brittle fracture. This K_{Ic} is called the fracture toughness. As illustrated in Figure 8-3, K_{Ic} is usually a function of material strength. Very importantly, it is also a function of the material or specimen thickness (Figure 8-4).

9 Delayed hydride cracking (Kit Coleman)

9.1 Introduction

Delayed Hydride Cracking (DHC) is a stable crack growth mechanism that has led to failures in Zr2.5Nb fuel cladding [Simpson & Ells, 1974] and pressure tubes [Perryman, 1978] and possibly in Zircaloy fuel cladding [Schrire et al, 1994], [Edsinger et al, 2000], [Sakamoto et al, 2008]. The cracking process consists of several steps:

- Hydrogen diffuses up a tensile stress gradient at a flaw tip where a hydrogen concentration gradient develops;
- If the hydrogen concentration exceeds the solubility limit, C_P, hydride precipitates nucleate;
- With time, the precipitates grow, and if the local tensile stress is large enough, the precipitates will crack once they reach a critical size;
- The process repeats itself leading to an average crack growth rate, V.

The cracking is an intermittent process. Although it is the hydride that cracks, it is the hydrogen that moves and it is this movement that causes the delay and controls the rate of cracking.

The temperature, T, dependence of V is complicated, illustrated schematically in Figure 9-1 [Cheadle et al, 1987]. Often ln(V) is plotted against 1/T to provide an Arrhenius-type of plot, and an activation energy for cracking related to the temperature dependence of hydrogen diffusivity and solubility limit. Care should be exercised in making such a plot and relating the data to the practical situation. Several limits to cracking lead to the complications as follows:

1) When attaining the test temperature by heating from T_1, a temperature is reached where V starts to decline, T_2, and with further heating cracking stops altogether at T_3. T_2 and T_3 depend on T_1.

2) When cooling from a high temperature where all the hydrogen is in solution, T_4, a temperature is reached, T_5, where cracking can start. T_5 depends on the hydrogen concentration through the solubility limit.

3) With further cooling, V passes through a maximum value at T_6, then declines with temperature as one would expect from the Arrhenius approach.

4) Testing at T_3 after cooling from a temperature between T_3 and the temperature when all the hydrogen is in solution, T_D, provides values of V ranging from zero up to the possible maximum values (Figure 9-2), [Shek & Graham, 1989], [McRae et al, 2010].

5) An upper temperature, T_U, exists above which cracking cannot take place despite having hydrides present and cooling to the test temperature from above T_D, Figure 9-3 [Sagat & Puls, 2003], [Resta Levi & Puls, 2005].

6) A further limitation is based on K_I. Up to a critical value, no cracking takes place. This threshold value is called K_{IH} [Coleman & Ambler, 1977], [Simpson & Puls, 1979]. Once K_{IH} is exceeded, after a narrow range of K_I in which V changes rapidly, V is usually almost independent of K_I until K_{IC} is approached (Figure 9-4). The value of K_{IH} is almost independent of temperature but starts to rise in association with T_U (Figure 9-4), [Resta Levi & Puls, 2005].

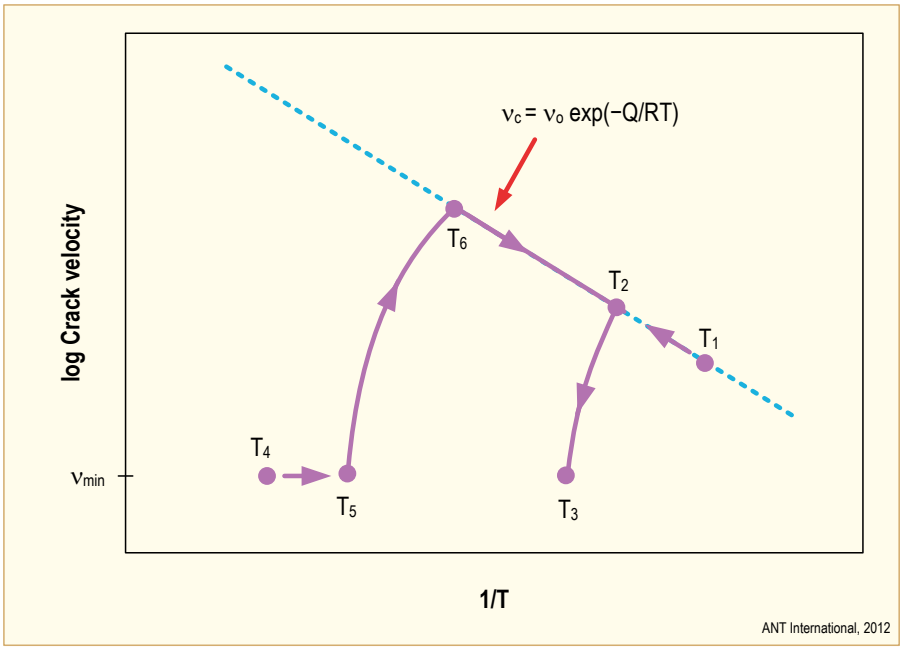

Figure 9-1: Schematic diagram of the temperature dependence of the DHC velocity, showing the effect of temperature history. On heating from T_1, the crack starts to slow at T_2 and stops at T_3, even if hydrides are present. (Both T_2 and T_3 have been called T_{DAT}, with T_3 being perhaps preferred.) On cooling from T_4, often when the hydrogen is all in solution, cracking starts at T_5; with further cooling V rises to a maximum value at T_6, then decreases following an Arrhenius relationship with temperature. (T_5 is sometimes called T_{RIT}.), after [Cheadle et al, 1987].

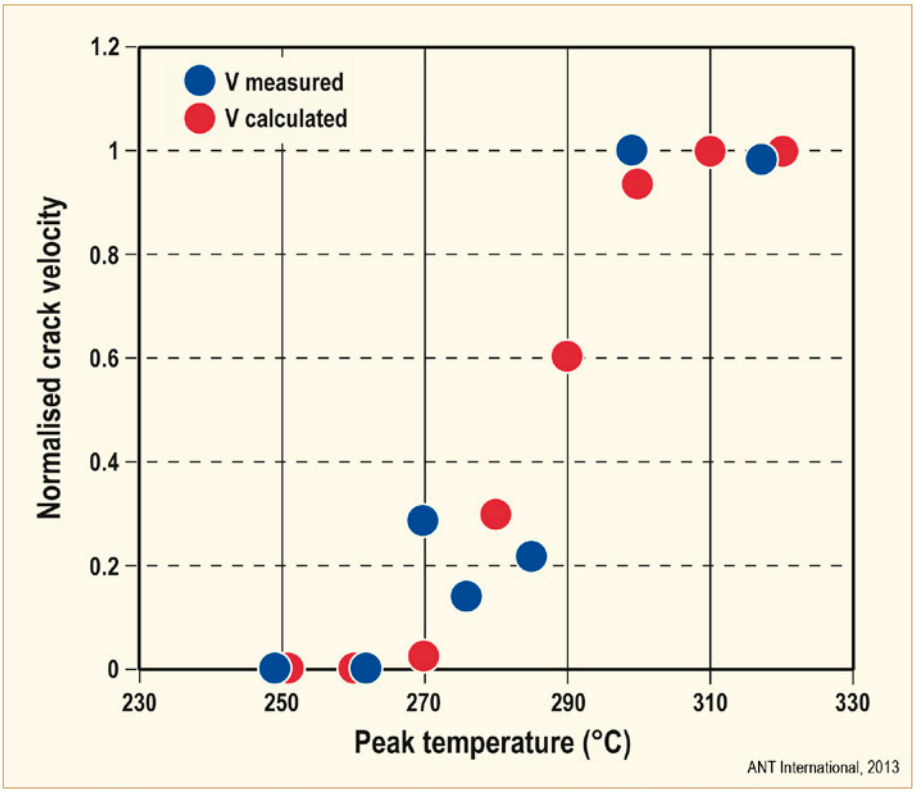

Figure 9-2: Demonstration of requirement that to attain maximum value of crack growth rate the peak temperature should exceed T_D [Shek et al, 2005]. Specimens of cold-worked Zr2.5Nb contained 60 ppm hydrogen that is all in solution above about 302°C and T_P is about 243 °C. Calculated values based on Diffusion First Model – Eq. 9-1, after [McRae et al, 2010].

10 Unusual tests (Tahir Mahmood)

10.1 SiC component testing techniques

10.1.1 Introduction

The post-Fukushima era has resulted in a significant level of nuclear industry interest in the development of Accident Tolerant Fuel (ATF). Based on the evidence from both Fukushima and TMI-2, the key to achieving accident resistance in commercial nuclear fuel is the fuel cladding, which is supposed to contain the fuel and the fission products as the first line of defence against release of fission products to the environment. During the accidents mentioned above, Zircaloy cladding lost all of its strength upon heating above 500°C and ballooned, blocking flow to the core interior, and cladding reacted exothermically with water releasing large quantities of heat and hydrogen gas. For Boiling Water Reactors, an additional source of the excessive heat and hydrogen release during the accident at Fukushima was the Zircaloy channel boxes, which comprise about half the volume of Zircaloy in the core, and hence released about half the heat and hydrogen during the hours following the accidental core uncover [Feinroth et al, 2013].

An alternative to Zircaloy cladding that does not react exothermically with water and release hydrogen when quenched at high temperatures is the ceramic material silicon carbide. Over several decades of research for fusion reactor materials in Japan and the US, it was learned that some forms of silicon carbide are radiation resistant and hence may be usable in fission reactors [Newsome et al, 2007]. Silicon carbide (SiC) composite, which is SiC matrix reinforced by SiC fibre, is one of the candidates of accident tolerant fuel (ATF) cladding material. Table 10-1 compares the relevant properties of zirconium alloys, stainless steel, and SiC for use as cladding material [Kitano et al, 2013].

Table 10-1: Comparison of Zirconium Alloys and ATF candidates, after [Kitano et al, 2013].

	Zirconium alloy	Stainless steel	SiC
Melting temperature	2100K	1700K	3000K
Phase transformation temp.	1100K (α to β)	900K (sensitization)	2500K (β to α)
High temperature oxidation (Hydrogen generation)	High rate	Low rate	Extremely low rate
SCC with water	No	Yes	No
Corrosion	High rate	Low rate	Low rate
Thermal neutron absorption cross-section	0.18b	2.9b	0.08b
Mechanical properties at operational temperature	High strength Medium ductility High toughness	High strength High ductility High toughness	High strength Improved ductility Improved toughness
Stability against irradiation	Good	Good	Good
ANT International, 2013			

The triplex SiC cladding is a three layer, all silicon carbide, tube that has almost the same dimensions as Zircaloy cladding in current LWRs [Feinroth et al, 2013], as shown in Figure 10-1. Each of the three layers fulfils a different design requirement. The inner high density monolith layer of stoichiometric beta phase SiC assures hermeticity and fission gas retention during normal operation and reactor transients. The middle layer is SiC fibre winding. The strength of the tube is improved by pre-tensioning the fibres. Such a tube could withstand very high internal fission gas pressure prior to breaching the inner monolith tube. A third dense outer layer of monolithic SiC is added to enhance water side corrosion resistance. As shown in the Figure 10-2 below, such silicon carbide composites retain their strength at temperatures of 1500°C, as compared to Zircaloy which loses most of its strength above 500°C. The high strength at high temperature assures survival of the triplex SiC cladding with minimum damage (fission gas release only) during LOCA events. The material is also expected to be resistant to failure during departure from nucleate boiling (DNB) transients, thus allowing an increase in power density, and power output. And because silicon carbide is very hard, it is expected to be resistant to operational fuel failures sometimes caused in zirconium alloy fuel rods by grid fretting and debris.

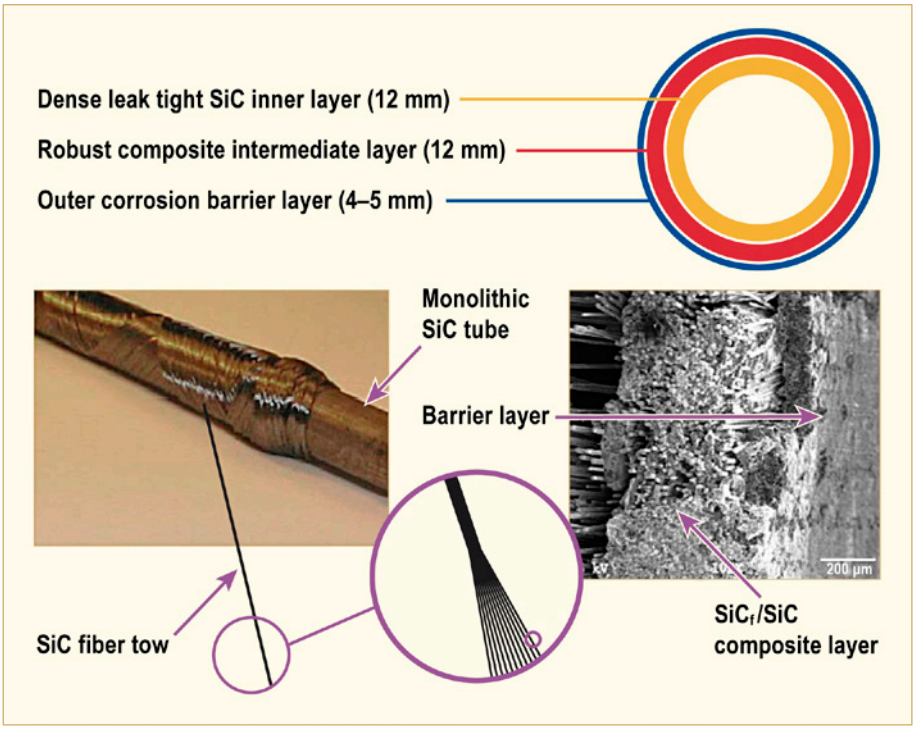

Figure 10-1: TRIPLEX™ fuel clad construction [Feinroth, 2012a].

11 Hydride effects (Ron Adamson)

11.1 Introduction

When hydrogen (H) is taken up during corrosion of zirconium alloys, or during special hydriding treatments, zirconium hydrides may be formed. Although hydrides exist as several different phases, in reactor application it generally occurs as delta (δ), $ZrH_{1.6}$. In tubing, hydrides occur as various mixes of circumferential (hoop or tangential direction) and radial (through-thickness) orientations, as illustrated in Figure 11-1.

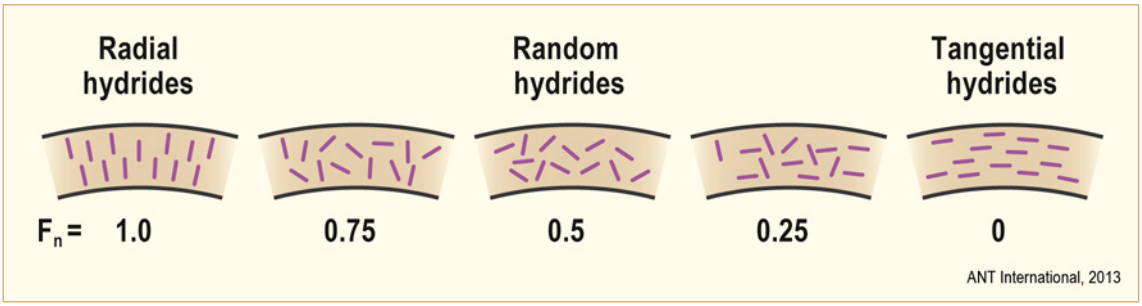

Figure 11-1: Typical hydride orientations observed in metallographic cross-sections of zirconium alloy cladding. "F" is a quantification of the degree of radial hydrides, after [Källström, 1975].

The two extremes are shown in Figure 11-2 [Chu et al, 2005]. In this figure, where the cross-section sample has been etched, the revealed hydrides appear to be long and continuous.

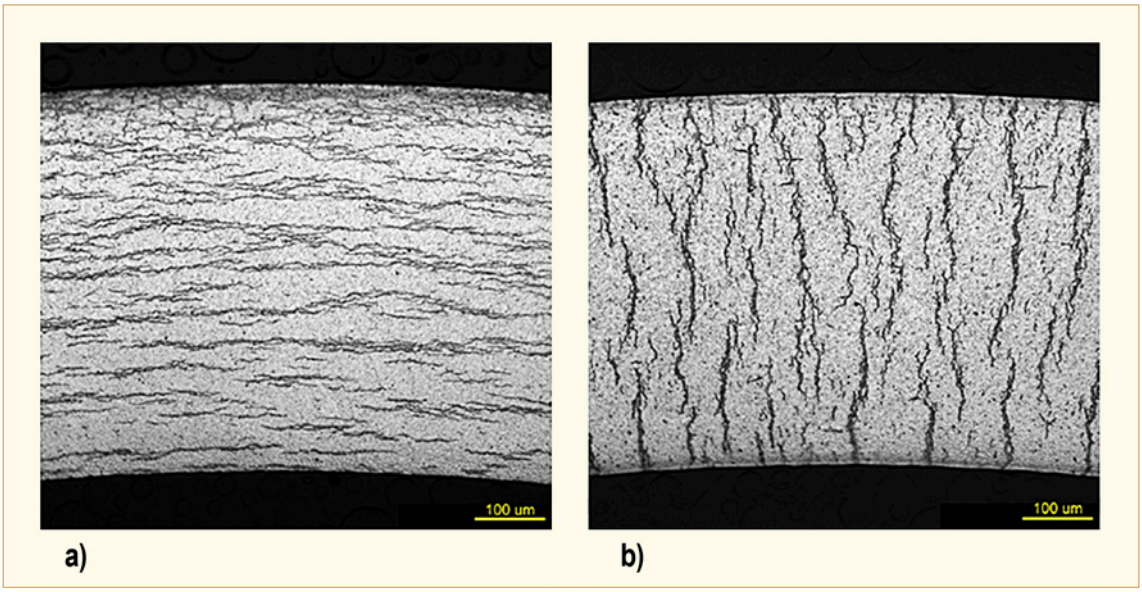

Figure 11-2: Examples of (a) circumferential and (b) radial hydride orientation [Chu et al, 2005].

In reality, the "long" hydrides consist of bundles of short hydrides on the order of micrometres (μm) in length lined up on planes near the basal (0001) orientation, illustrated in Figure 11-3 and Figure 11-4 [Chung et al, 2002].

Hydrides in zirconium alloy tend to have alignment near the basal plane, but also form on grain boundaries, dislocations (including loops) and previously existing hydrides. Cooling rate during formation has a strong influence on size and distribution, as shown in Figure 11-5 [Ells, 1968].

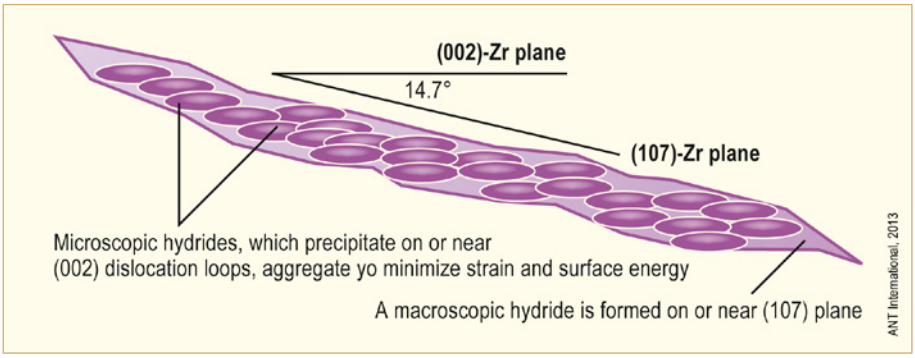

Figure 11-3: Schematic illustration of micrometre size hydrides bundling up to form the long hydride image when the metallographic section is etched, after [Chung et al, 2002].

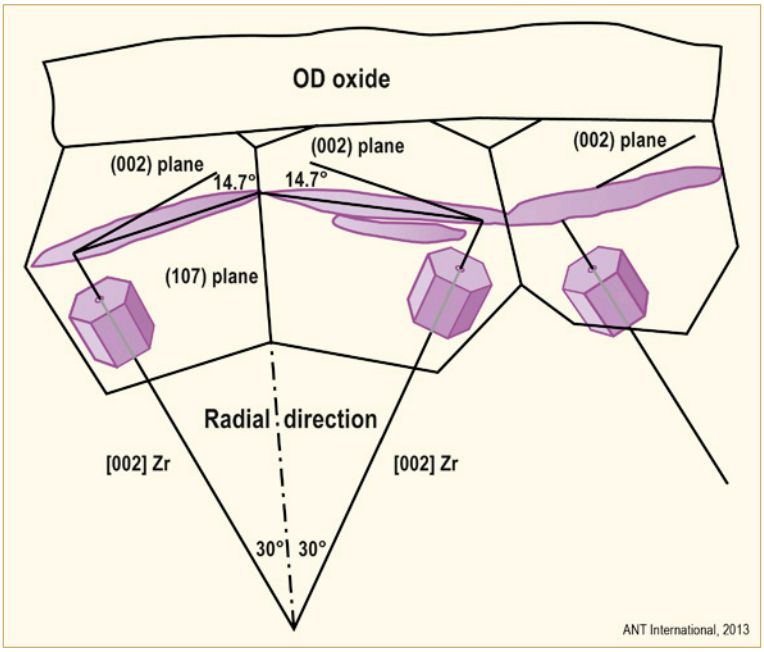

Figure 11-4: Schematic illustration of short hydrides making up stringers closed aligned in slightly different (zigzag) orientation, after [Chung et al, 2002].

12 References

10 CFR Part 50 Appendix A, *General Design Criteria for Nuclear Power Plant*s, US, Government Printing Office, Washington, 1990.

10 CFR Part 100, NRC, Standard Review Plan, NUREG-0800, USNRC, 1995.

Adams B. L. and Murty K. L., Mat. Sci. Eng., Vol. 70, pp. 181-190, 1985.

Adamson R. B. and Bell W. L., *Effects of Neutron Irradiation and Oxygen Content on the Microstructure and Mechanical Properties of Zircaloy*, Microstructure and Mechanical Behaviour of Materials, Proceedings: Int'l Symposiums, Xian, China, October, 1985, EMAS, pp. 237-246, Warley, UK, 1986.

Adamson R. B., *Cyclic Deformation of Neutron Irradiated Copper*, Phil. Mag. 17, pp. 681, 1968.

Adamson R. B., Wisner, S. B., Tucker, R. P. and Rand. R. A., *Failure Strain for Irradiated Zircaloy Based on Subsized Specimen Testing and Analysis*, The Use of Small-Scale Specimens for Testing Irradiated Material, ASTM STP 888, W. R. Corwin and G. E. Lucas, Eds., American Society for Testing and Materials, 171-185, Philadelphia, 1986.

Adamson, R. B. and Lewis, J. L., Abstracts, Ninth International Symposium, Zirconium in the Nuclear Industry, Kobe, Japan, 1991.

Adamson R. B., *Effects of Neutron Irradiation on Microstructure and Properties of Zircaloy*, Zirconium in the Nuclear Industry; Twelfth International Symposium, ASTM STP 1354, pp. 15-31, West Conshohocken, PA, 2000.

Adamson R. B., *Recovery of Irradiation Damage by Posts-Irradiation Thermal Annealing-Relevance to Hydrogen Solubility and Dry Storage Issues*, EPRI Technical Report 1013446, June 2006.

Adamson R., Cox B., Davies J., Garzarolli F., Rudling P. and Vaidyanathan S., *Pellet-Cladding Interaction (PCI and PCMI), ZIRAT11/IZNA6*, Special Topics Report, ANT International, Mölnlycke, Sweden, 2006/2007.

Adamson R. B, Garzarolli F. and Patterson C., *In-Reactor Creep of Zirconium Alloys*, ZIRAT14/IZNA9 Special Topical Report, ANT International, Mölnlycke, Sweden, 2009.

Adamson R. B, Garzarolli F., Patterson C., Rudling P. Strasser A. and Coleman K., *ZIRAT15/IZNA10 Annual Report*, ANT International, Mölnlycke, Sweden, 2010.

Ahn J. H. and Kwon D., J. Mater. Res. 16 3170, 2001.

Alam A. and Hellwig C., *Cladding Tube Deformation Test for Stress Reorientation of Hydrides,* Journal of ASTM International, Vol. 5, No. 2, Paper ID JAI101110, 2009.

Alvarez-Armas I and Herenu S., *Influence of dynamic strain aging on the dislocation structure developed in Zircaloy-4 during low-cycle fatigue*, J. Nucl. Mater., Vol. 334, pp. 180-188, 2004.

Ambler J. F. R., *The effect of temperature on the micro-indentation properties of zirconium Hydride*, Atomic Energy of Canada, Report, AECL-2538, 1966.

Amzallag C., *Environment Assisted Fatigue of Stainless Steels in PWR Environment*, ANTI LCC6 Seminar, 2011.

Anghel C., Alvarez Holston A. M., Lysell G., Karlsson S., Jakobsson R., Sund E., Mahmood S. T., *An Out-of-Pile Method to Investigate Iodine-induced SCC of Irradiated Cladding*, Proceedings of the Top Fuel conference, Paris, France, 2009.

Anonymous, *Standard test method for determining threshold stress intensity factor for environment-assisted cracking of metallic materials*, ASTM Standard E1681-03, 2003. (Reapproved 2008)

Anonymous, *Standard specification for wrought zirconium and zirconium alloy seamless and welded tubes for nuclear service (except nuclear fuel cladding)*, ASTM International, B353-07, Revised 2007a.

Anonymous, *Standard specification for wrought zirconium alloy seamless tubes for nuclear reactor fuel cladding*, ASTM International, B811-07, Approved 2007b.

Anonymous, *Standard Specification for Wrought Zirconium and Zirconium Alloy Seamless and Welded Tubes for Nuclear Service (Except Nuclear Fuel Cladding)*, ASTM B353 – 12, Re-approved 2012.

Anonymous, Standard Specification for Wrought Zirconium Alloy Seamless Tubes for Nuclear Reactor Fuel Cladding, B811 – 13, Re-approved 2013.

Antolovich S. D., *An Introduction to Fracture Mechanics*, ASM Handbook – Fatigue and Fracture, Vol.19, pp. 371-380, 1997.

Aomi M., Baba T., Miyashita T., Kamimura K., Yasuda T., Shinohara Y., and Takeda T., *Evaluation of Hydride Reorientation Behaviour and Mechanical Properties for High-Burnup Fuel- Cladding Tubes in Interim Dry Storage*, Journal of ASTM International, Vol. 5, Issue 9, Paper ID JAI101262, 2009a.

Aomi M. et al, *The Hydrogen Pick-up Behaviour for Zirconium-based Alloys in Various Out-of-pile Corrosion Test Conditions*, Top Fuel 2009, Paper 2077, Paris France, 2009b.

Armas A. F. and Alvarez-Armas I., *Cyclic Behavior or Zircaloy-4 at Elevated Temperatures*, Zirconium in the Nuclear Industry: Seventh Int'l Symposium, ASTM STP 939, R. B. Adamson and L. F. P. Van Swam, Eds., Am. Soc. for Testing and Materials, Philadelphia, 617-630, 1987.

Armas A. F., Herenu S., Bolmaro R., and Alvarez-Armas, I., *Cyclic softening mechanisms of Zircaloy-4*, J. Nucl. Mater., Vol. 326, pp. 195-200, 2004.

Arséne S. and Bai J. B., *A new approach to measuring transverse properties of structural tubing by a ring tes*t, Journal of Testing and Evaluation, JTEVA, Vol. 24, No. 6, pp. 386-391, 1996.

ASME, *Rules for Construction of Nuclear Power Plants Components*, ASME Boiler and Pressure Vessel Code, Section III, 2010.

ASTM Standards E328-02, Section 3, Vol. 0.3.01; *Methods – Mechanical Testing E 328-86 Standard Method for Stress Relaxation Tests for Materials and Structures*, (Reapproved 2008), 2010.

ASTM Standard E4, *Standard Practices for Force Verification of Testing Machines*, 2013.

ASTM Standard E8/8M, *Standard Test Methods for Tension Testing of Metallic Materials*", 2013.

ASTM Standard E9, *Standard Test Methods of Compression Testing of Metallic Materials at Room Temperature*, 2013.

ASTM Standard E18, Standard Test Methods for Rockwell Hardness of Metallic Materials, 2013.

ASTM Standard E83, *Standard Practice for Verification and Classification of Extensometer Systems*, 2013.